Fenton Hill Revisited: The Retention of Helium in Zircons and the Case for Accelerated Nuclear Decay

Gary H. Loechelt*

September 11, 2008

Abstract

A young-earth creationist research program, called RATE for Radioisotopes and the Age of The Earth, claims to have found scientific evidence for the acceleration of nuclear decay rates by several orders of magnitude. This argument is used to defend their belief in a 6000-year-old earth. One of their most celebrated case studies involves the helium retention in zircons ($ZrSiO_4$ crystals) from geothermal test wells at Fenton Hill, New Mexico. When the scientific merits of the Fenton Hill study are examined, five specific flaws in the data analysis and modeling are found which are serious enough to invalidate the argument for accelerated nuclear decay. Furthermore, once these errors are corrected, forward modeling of the helium diffusion from these zircons produces retention values that are commensurate with the radiometric ages of the samples. Therefore, not only is the accelerated nuclear decay argument invalidated, but the scientific evidence supports the conventional 4.5 billion year age of the earth.

1. Introduction

Radiometric dating methods have long been a target of young-earth creationists, and for good reason. The strongest line of evidence supporting the commonly accepted 4.5 billion year age of the earth is the radiometric dating of rocks and minerals using long-lived radioactive nuclei. Rock ages obtained by these dating methods, usually ranging from millions to billions of years, directly contradict belief in a 6000-year-old earth.

For many years, the young-earth community has been content to use the tactics of trying to discredit radiometric dating altogether, claiming that fatal flaws invalidate the method and that the isotopic patterns which are widely observed today in rocks and minerals can be explained by other non-nuclear processes in the earth (Cook, 1968; Slusher, 1973; Morris, 1974; Helmick and Baumann, 1989; Austin, 1994; Morris, 1994; Gill, 1996; Austin and Snelling, 1998; Woodmorappe, 1999). A logic consequence of this position requires that very little nuclear decay has occurred since the formation of the earth.

Two fundamental flaws are usually seen in these arguments. First, they fail to demonstrate in the common case that experimental uncertainties result in errors of sufficient magnitude to completely invalidate the dating methods in question. Second, and perhaps more importantly, no credible alternative is given which can adequately explain the well-documented patterns in isotopic ratios which are repeatedly observed in terrestrial, lunar, and meteoric samples (Dalrymple, 1991).

Perceiving this weakness in the young-earth position, a group of prominent scientists from Institute for Creation Research and the Creation Research Society (Dr. Steve Austin, Dr. John Baumgardner, Dr. Eugene Chaffin, Dr. Don DeYoung, Dr. Russell Humphreys, and Dr. Andrew Snelling) met to discuss the "problem" with radiometric dating. (Vardiman *et al.*, 2000. See in particular the discussion beginning on p. 3.) The ensuing eight-year research program, called RATE for Radioisotopes and the Age of The Earth, acknowledged that much larger quantities of nuclear decay have occurred in most geologic processes than could be explained by an earth only a few thousand years old (Vardiman *et al.*, 2005; DeYoung, 2005). In effect, young-earth creationists of the 21st century finally accepted what mainstream science had known since the early 20th century, namely that nuclear decay was the best and perhaps only viable explanation for the isotopic patterns observed in rocks and minerals today, as well as other related phenomena, such as radiohalos and fission tracks.

Conceding the occurrence of billions of years' worth of nuclear decay created a major dilemma for people believing in a 6000-year-old earth. Since questioning a young-earth position was unthinkable (DeYoung, 2005, p. 174), the only remaining alternative was to postulate that nuclear decay rates were accelerated by many orders of magnitude in the recent past. The goal of the RATE project was to find scientific evidence to this end.

To test the hypothesis, researchers sought cases in which nuclear decay could be compared against some other natural phenomenon. Think of a radioactive nucleus as a clock that ticks (*i.e.* decays) at a known rate. The only way to demonstrate that nuclear processes "ticked" faster in the past was to compare their decay rates to another, more accurate clock. Most of the cases documented by the RATE team proved to be weak tests for their hypothesis because the other clocks were not independent (*i.e.* they were also based upon nuclear phenomena) and showed very little difference in time (*i.e.* 10-20% instead of 5-6 orders of magnitude).

The notable exception was a helium diffusion experiment using zircon mineral samples ($ZrSiO_4$ crystals) from deep geothermal test wells at Fenton Hill, New Mexico. The RATE team claimed that when they compared the nuclear decay clock with their helium diffusion clock, they found a large discrepancy (Humphreys, 2000 and 2005a; Humphreys *et al.*, 2003a, 2003b, and 2004; hereafter collectively referred to as Humphreys). Apparently, the nuclear decay clock recorded an elapsed time of over a billion years, whereas their helium diffusion clock recorded an elapsed time of only a few thousand years. Taking the helium diffusion time as the more reliable measurement, the researchers claimed that they had found convincing evidence for accelerated nuclear decay.

However, this apparent result is not as simple as merely reading time from a stopwatch. The helium diffusion clock used by the RATE team was actually a complex mathematical model describing the process of helium diffusion from zircon crystals. One may legitimately ask, "How well did they read their diffusion clock?"

After following their research for many years, I conclude that they read this clock poorly. The RATE

study contained at least five specific flaws in the data analysis and modeling that were serious enough to invalidate their conclusions. The deeper question still remains, though, as to whether the existing data can be reconciled within the context of an old earth. Forward modeling of the helium diffusion can provide the answer. This paper demonstrates that once the errors in the RATE diffusion model are corrected, both the nuclear decay clock and the helium diffusion clock are in excellent agreement. Therefore, the helium diffusion experiment cited by the RATE team actually supports an *old earth*. First, however, a review of the accelerated nuclear decay argument is in order.

2. The RATE argument

Los Alamos National Laboratories drilled deep wells into the Precambrian basement rock at Fenton Hill, New Mexico as part of the geothermal energy program. In the course of this work it was noted by researchers that significant amounts of helium remained in zircon crystals taken from well core samples despite the high temperature of their surroundings (Gentry *et al.*, 1982a). This phenomenon was explored in greater depth by the RATE research team from which they drew two conclusions. First, the presence of helium in the zircons suggests that significant amounts of radioactive decay have occurred in the past. Second, the retention of helium at the currently measured temperatures indicates that these zircons could not have remained at these temperatures for more than thousands of years, much less than the conventionally assigned Precambrian age of approximately 1.5 billion years.

The amount of helium in these zircon crystals was measured from core samples taken at several depths from the Fenton Hill drill holes. Using previous measurements of the lead content as an indicator of the total amount of alpha decay, the helium retention ratio was calculated after making a correction for the immediate loss due to α-ejection (Gentry *et al.*, 1982a). The additional loss of helium in these samples was attributed to solid state diffusion, which would be expected at the elevated temperatures measured down the wells.

The helium diffusivity in these zircons was then determined using two independent methods. First, an empirical diffusivity was measured using a conventional stepwise heating experiment. This result was compared to model diffusivities which were calculated from the helium retention data. Two models were considered: a young-earth creation model which assumed a total diffusion time of 6000 years and an old-earth uniformitarian model which assumed a total time of 1.5 billion years (Humphreys, 2000 and 2005a; Humphreys *et al.*, 2003b and 2004).

Under the various assumptions made, the diffusivity predicted by the young-earth model agreed favorably with the measured diffusivity whereas the prediction of the old-earth model disagreed by several orders of magnitude. Based upon these results the claim was made that the earth cannot be more than several thousands of years old and that periods of accelerated nuclear decay must have occurred in the recent past.

3. Errors in the RATE study

Although the impact of various physical effects, such as differences in chemical potential, gas solubility, and interface resistance, has been discussed at length (Humphreys *et al.*, 2004; Humphreys, 2005a), the robustness of the predicted helium retention to other factors deserves further consideration. In particular, there are five specific errors that were committed by Humphreys and his RATE colleagues in their helium diffusion modeling, two of which are serious enough to completely invalidate their conclusions. These five errors are expounded in the following discussion.

3.1. Helium retention measurements

The first error traces back to the prior work by Robert Gentry and his original estimate of the helium retention ratio. The helium retention is defined as the ratio of the measured quantity of helium released from a sample after heating (Q) to the total amount of helium generated from the α-decay of radioactive nuclei (Q_o). The volume of released gas was measured by Oak Ridge National Laboratory from zircon samples taken at six different depths from the Fenton Hill wells. (Gentry *et al.,* 1982a. See the references of Humphreys *et al.,* 2003b for corrections; also in Table I of Humphreys, 2005a.) These data are presented in Table 1 along with two additional measurements taken in the course of the RATE study (Humphrey *et al.,* 2003b and 2004).

In general, a continuous decline in the amount of helium was observed with depth, as would be expected. However, the two deepest samples had identical helium content despite the temperature difference between them. It is quite possible that in these two samples the background helium concentration of the surrounding host rock was being measured and not the helium generated from α-decay within the crystal itself. In support of this interpretation, the authors noted that the gas released from these two deepest samples came in short bursts of 1-2 seconds as opposed to the other samples, which liberated their helium over a span of more than 20 seconds. This release pattern suggested that the helium might be from an extrinsic source. Taking these factors into consideration, the conservative interpretation is to regard the helium as mostly depleted below a depth of 2900 m (197 ºC current well temperature) and measurably retained at and above this depth.

The problem with this helium retention experiment, however, was not in the *measurement* of the current helium content of these zircon samples, but in the *calculation* of the total amount of helium generated from the α-decay of radioactive nuclei (Q_o). This quantity was estimated using the ~80 ppm lead concentration measured at 2900 m, which was assumed to be representative of all the samples in the formation, regardless of depth. This assumption is not very good.

The Precambrian basement rock type at Fenton Hill changes with depth over a scale of kilometers from gneiss to gneiss with mafic schist to biotite granodiorite and back to gneiss. Furthermore, dozens of cores from the Precambrian section showed a marked diversity of composition, texture, degree of alteration, and fracturing over distances of only a few centimeters (Laughlin *et al.,* 1983). In fact, variations in the radioisotope content, or zoning, frequently occur in the zircon crystals themselves over a length scale of microns (Gentry *et al.,* 1982b). Because of effects like these, current researchers active in the (U-Th)/He thermochronometry field typically follow the practice of measuring both the He and U-Th content from the same sample (Reiners *et al.*, 2004). Unfortunately, this practice was not followed.

Far more seriously, even if the ~80 ppm lead concentration is assumed to be a valid measure of the amount of radioactive decay in these zircons throughout the depth of the formation, one still cannot account for the ~15 ncc/μg value for Q_o which was originally reported by Gentry and subsequently used in the RATE study. Since neither Gentry nor Humphreys have published details as to how they determined Q_o, this discrepancy remains unexplained.

Table 1
Helium retention ratios for zircons at various depths from geothermal test wells at Fenton Hill, NM. Samples #1-#6 are from Gentry *et al.,* 1982a; sample #2002 is from Humphreys *et al.,* 2003b; and sample #2003 is from Humphreys *et al.,* 2004. Borehole depth and current well temperature for each sample are given, along with the measured quantity of gas (Q) liberated after heating. The total amount of helium generated by nuclear decay (Q_o) was calculated using Eq. (1). See the example given in Eq. (2) for the value of several constants. Revised helium retention ratios (Q / Q_o) were calculated from these data. The original RATE ratios reported by Gentry and later Humphreys are shown for comparison. (See the references of Humphreys *et al.,* 2003b, regarding errors in Gentry *et al.,* 1982a.) Unlike the RATE values, the revised ratios do not include a correction for α-ejection in the denominator.

Sample	Depth (m)	Temperature (ºC)	Q (ncc/μg)	Q / Q_o (revised)	Q / Q_o (RATE)
2002	750	96	~12.1	~16%	~80%
1	960	105	8.6	12%	58%
2003	1490	124	6.3	8.6%	42%
2	2170	151	3.6	4.9%	27%
3	2900	197	2.8	3.8%	17%
4	3502	239	0.16	0.2%	1.2%
5	3930	277	~0.02	~0.03%	~0.1%
6	4310	313	~0.02	~0.03%	~0.1%

For the sake of discussion, a brief description of the relevant equations is given here. The total volume of helium gas at standard temperature and pressure (STP) resulting from the α-decay of radioactive nuclei can be calculated from either the lead concentration or from the U-Th concentrations and the age of the sample using the following formula:

$$Q_o = N_\alpha \left(\frac{P}{RT}\right)^{-1} \left(\frac{C}{M}\right). \quad (1)$$

Here Q_o is the volume of helium gas at STP, N_α is the number of α-particles emitted in the decay chain, R is the molar gas constant (8.314472 J/mol/K), T and P are standard temperature and pressure respectively (273.15 K and 101325 Pa, from Baum *et al.,* 2002), C is the mass concentration of decayed atoms, and M is the corresponding atomic mass. The constant P/RT evaluates to 44.615 μmol/cc. The concentration of decayed atoms can be determined from either the daughter isotope or the parent isotope if the sample age is known (Dickin, 1995). For the U and Th decay series, there are 8 α-particles emitted by ^{238}U, 7 by ^{235}U, and 6 by ^{232}Th.

For the case in question, the concentration of the daughter isotopes was 80 ppm with ^{206}Pb:^{207}Pb:^{208}Pb ratios of 10:1:1. Using 7.75 as a mean value for N_α and 206.22 as a mean value for M, Eq. (1) reduces to

$$\begin{aligned} Q_o &= \frac{7.75 \times 80 \times 10^{-6}}{206.22\,\mu g/\mu mol \times 44.615\,\mu mol/cc} \\ &= 6.739 \times 10^{-8}\ cc/\mu g \\ &= 67.39\ ncc/\mu g\,. \end{aligned} \quad (2)$$

The Oak Ridge research team proceeded to correct this quantity for near-surface α-ejection. Unfortunately, the method for this correction was neither documented nor referenced. Subsequent researchers have published their own correction formulas (Farley, 2002). A better approach, however, is to self-consistently account for α-ejection during diffusion (Meesters and Dunai, 2002b). It is worth noting that an α-particle loss of 30-40% was estimated for the smaller zircons (Gentry *et al.,* 1982a). This range is consistent with a loss of 40% for a 30 μm sphere calculated using the method of Farley. Taking 40% as an upper limit, the minimum corrected value for Q_o would be around 40 ncc/μg, which is well over twice the value of ~15 ncc/μg reported by Gentry and subsequently used in the RATE study. Humphreys maintains that the original calculations are correct, despite unpublished criticism. However, he has yet to provide an explanation as to how a helium content of only ~15 ncc/μg was determined (Humphreys, 2005b).

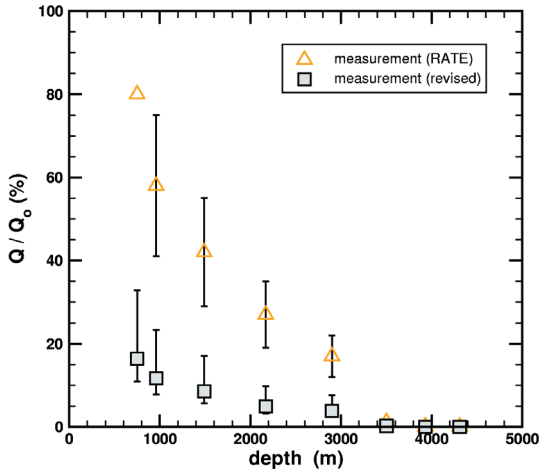

Figure 1. Helium retention ratios versus geothermal well depth. A comparison is made between the original RATE measurements reported by Gentry and Humphreys and the revised measurements calculated in this paper. The error bars on the revised measurements are estimates only, and do not reflect a rigorous statistical treatment. They were calculated by assuming a ±50% variation in the total amount of helium generated from the α-decay of radioactive nuclei (Q_o).

A further compounding problem is the use of the lead concentration in the zircons as a proxy for the total amount of α-decay. Based upon a detailed isotopic analysis, Zartman (1979) concluded that the lead system showed signs of redistribution at the mineral grain level, even though no evidence for disturbance was found at the whole rock level. Using his measured concentrations of 328.78 ppm for uranium and 169.42 ppm for thorium and a decay time of 1440 Ma, a Q_o value of 73.68 ncc/μg is obtained. This number will be used in the subsequent analysis instead of the original Q_o value calculated by the Oak Ridge research team, with the correction for α-ejection being handled during the diffusion simulations (Meesters and Dunai, 2002b).

Table 1 summarizes my revised estimate of the helium retention ratios versus depth at Fenton Hill. The RATE numbers of Gentry and Humphreys are also given for comparison. These data are also plotted in Fig. 1 as a function of depth. Note that the revised ratios do not include any correction for α-ejection in the denominator because this effect is

handled self-consistently in the diffusion algorithm that is described later in the paper.

3.2. Physical geometry

The remaining errors committed by the RATE researchers all pertain to their diffusion model. This model comprises several components, including a physical geometry, surface boundary conditions, thermal history, and material properties. Remarkably, the RATE team managed to make mistakes in all four of these areas. The physical geometry will be addressed first.

Zircon crystals typically form in the shape of tetragonal prisms with a relatively high aspect ratio (length-to-width) of 2:1 or greater. A rigorous diffusion model would use a realistic 3-dimensional geometry. It has been demonstrated through direct computation, however, that a simpler spherical geometry is a reasonably good approximation *provided* the effective radius is chosen such that the surface-to-volume ratio of the sphere is the same as the real geometry (Meesters *et al.,* 2002a).

The zircons used in the RATE study of Fenton Hill had sizes ranging from 50-75 μm in total length (Humphreys *et al.*, 2003b and 2004; Humphreys, 2005a). Taking 67 μm as a typical median size, a zircon crystal with a 2:1 aspect ratio has the same surface-to-volume ratio as a 20 μm sphere. (Farley, 2002, caption of Table I. Detailed calculations are given below.) The RATE team, on the other hand, using a mean half-length criterion instead of the surface-to-volume ratio, chose a much larger radius of 30 μm. Interestingly enough, Humphreys had calculated a radius of 22 μm in an earlier work by matching the surface areas of the zircons to equivalent spheres (Humphreys, 2000). The radius used in this earlier work is much closer to the correct value and is based upon better physical reasoning. The implications of increasing the model radius from 22 μm to 30 μm will be discussed later, along with possible reasons why the RATE team made this change.

For a tetragonal prism, which is the typical shape of most zircon crystals, the surface-to-volume ratio can be approximated as

$$\beta = \frac{4LW + 2W^2}{LW^2} = \frac{4\left(L/W\right) + 2}{L}, \qquad (3)$$

where L is the prism length and W is the prism width. If a 2:1 aspect ratio is assumed for the length and width, Eq. (3) reduces to only one variable,

$$\beta = \frac{10}{L} = \frac{10}{67\,\mu\text{m}} = 0.15\,\mu\text{m}^{-1}. \qquad (4)$$

This surface-to-volume ratio, corresponding to a crystal with length of 67 μm, is typical of the size used by both Gentry and Humphreys in their experiments. The equivalent equation for a sphere of radius a is

$$\beta = \frac{3}{a} = \frac{3}{20\,\mu\text{m}} = 0.15\,\mu\text{m}^{-1}. \qquad (5)$$

Hence, a 20 μm sphere, which has the same β value, is the appropriate equivalent geometry for the real crystals.

A concrete example regarding the calculation of the spherical radius might be helpful here. Humphreys published an SEM picture of a representative zircon from his 2003 sample group (Humphreys, 2005a, Figure 11). Based upon the 20 μm calibration scale, the length of the crystal is about 70 μm and the width only 30 μm. An out-diffusing atom will, on average, take the shortest path of escape, not the longest. If this crystal is representative of his sample, then 30 μm is a bad choice for the effective spherical radius. A helium atom that diffuses 30 μm could possibly enter through one side of the crystal and leave the other! By comparison, Eq. (3) gives a surface-to-volume ratio of 0.16 μm^{-1}, which agrees well with the value of 0.15 μm^{-1} calculated in Eqs. (4)–(5). This ratio corresponds to an effective spherical radius of 18.5 μm, which is fairly close to 20 μm.

Larger radii bias the diffusion simulations to higher retention values. Simulations with smaller zircons result in lower retention values since over half the helium atoms leave the crystal by α-particle ejection before any diffusion can occur. Consequently, this error in the physical geometry had the effect of artificially *increasing* the helium retention ratios predicted by the RATE models. It is curious to note that even their young-earth model needed some kind of assistance in order to match the measured data. Evidently, another error is lurking in the background.

3.3. Surface boundary conditions

The rate at which diffusing helium atoms can leave a zircon crystal depends upon the environment in which the crystal is embedded. In many rocks, zircons are often found inside larger biotite crystals. The RATE researchers assumed that this was the case in their Fenton Hill study.

In their published papers, the RATE team discuss a diffusion model by Bell (1945) which is capable of handling a system of two concentric spheres with different diffusion coefficients (Humphreys *et al.*, 2003b; Humphreys, 2005a). Although the authors imply that this model is well suited for modeling the two material zircon/biotite system, they never actually use the model! Instead, they use a simpler model in which both materials have the same diffusion coefficients. The justification given for this simplification, despite the fact that the diffusivity of helium in biotite is much higher than that of zircon, is that "this approximation is generous to the uniformitarian point of view because it increases the time helium could remain in the zircons." (Humphreys, 2005a, p. 49) Yet, in a classic bait and switch maneuver, this approximation is applied only to their young-earth creation model, and not to their old-earth uniformitarian model. In the old-earth model, the effect of the surrounding biotite is neglected altogether (Humphreys *et al.*, 2003b, p. 184; Humphreys, 2005a, p. 53).

Given these conflicting remarks, it is fair to ask "What is the relationship between the diffusivity of helium in biotite to that of zircon?" Although the raw diffusion data for these two materials were published by the RATE team (Humphreys *et al.*, 2003b and 2004; Humphreys, 2005a), they were never actually compared. For reference, a graphical comparison is made here in Fig. 2 using an effective radius of 44 µm for biotite (based on the quoted size range of 75-100 µm) and 20 µm for zircon (see section 3.2).

From this figure it is apparent that below 300 °C, which is the temperature region of interest, the diffusivity of helium in biotite is 2-3 orders of magnitude higher than that of zircon. Essentially, once a helium atom diffuses to the zircon/biotite interface, little impedance to its further migration is offered by the surrounding biotite. A more appropriate boundary condition would require the helium concentration to approach zero at the zircon surface, instead of treating the zircon/biotite boundary as an interface between two materials with identical diffusion properties.

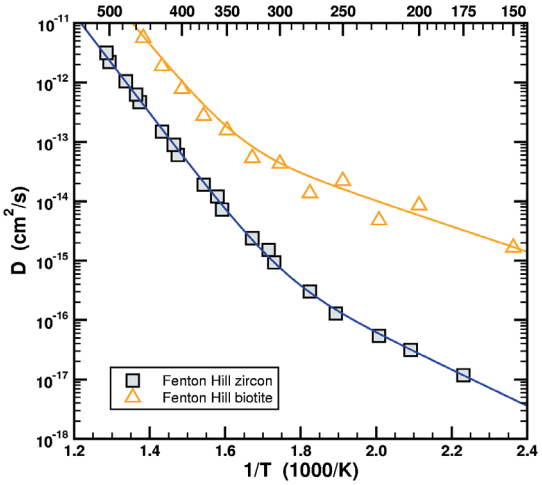

Figure 2. Arrhenius plot of the helium diffusivity in biotite and zircon, using an effective radius of 44 µm for biotite and 20 µm for zircon. Both mineral samples were taken from the Fenton Hill wells.

Even though the RATE researchers used this zero concentration boundary condition for their old-earth uniformitarian model, they chose an equal helium diffusivity boundary condition for their young-earth model. They were well aware that this choice had the effect of increasing the time helium could remain in the zircons. As in the case for the physical geometry, we encounter an error which effectively *increases* the helium retention for the young-earth model. One may well wonder why a model which only has to demonstrate helium retention for 6000 years requires so much artificial assistance. Perhaps it is compensating for a more fundamental flaw in the whole approach? This topic will be addressed later in the paper.

As an aside, it is worth noting a logical inconsistency that is pervasive throughout young-earth creation literature in general. Quite often, young-earth creationists propose point theories to solve isolated anomalies. By that I mean these theories often contain features which apparently solve a given problem, but fail when generalized to a wider range of phenomena. Here is a good example. Another case study cited by the RATE team is the existence of polonium radiohalos in granites (Snelling *et al.*, 2003a and 2003b; Snelling, 2005).

The RATE radiohalo theory proposes the following mechanism for the formation of polonium radiohalos. Radon gas escapes uranium bearing minerals, such as zircon, which are embedded in biotite crystals, and migrates to accumulation sites where it decays into polonium, thereby forming a radiohalo. This theory requires that the heaviest of all noble gases, radon, have the ability to leave its host mineral and travel scores of microns between biotite plates, all within the time constraint determined by the 3.8235 day half-life of ^{222}Rn. On the other hand, the helium diffusion theory requires that this same biotite trap helium, the lightest of all noble gases, and hold it for thousands of years. Clearly, the RATE researchers were focused on two isolated phenomena (helium diffusion and radiohalos) rather than solving a more general problem, like noble gas migration in biotite. Ironically, the helium diffusion study and the polonium radiohalo study are published as consecutive chapters in the same book (Humphreys, 2005a and Snelling, 2005).

3.4. Thermal history

All things considered, the errors mentioned up until this point are somewhat inconsequential to the ultimate question regarding the accelerated nuclear decay hypothesis. Although they demonstrate deficiencies in the RATE study, they cannot account for the several orders of magnitude discrepancy between their old-earth uniformitarian model and measured data. In contrast, the remaining two errors are far more serious and are of sufficient magnitude to invalid the conclusions of the Fenton Hill helium diffusion study.

The first of these major errors in the RATE study is the use of a constant temperature profile in their old-earth uniformitarian model. The original purpose of the deep wells drilled at Fenton Hill was to study the suitability of this site for extracting geothermal energy. Recent volcanic activity has raised the geothermal gradient in the area (the rate at which temperature increases with depth in the earth) to over twice its typical value in continental crust. These elevated temperatures have been sustained for a relatively short period of time on a geologic timescale. The use of a constant temperature over time by the RATE team demonstrates their misunderstanding of the thermal history of the site as well as the meaning of the word “uniformitarian”.

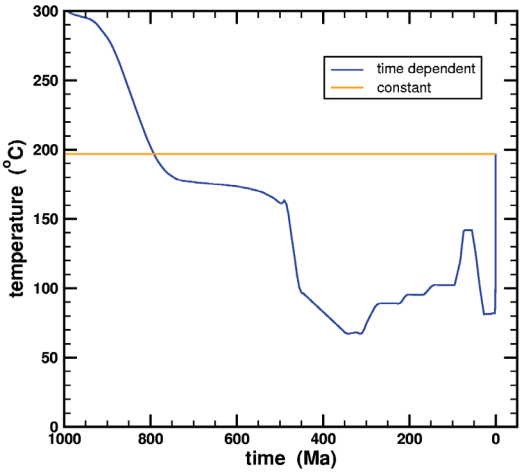

Figure 3. Comparison of the constant temperature profile used in the RATE uniformitarian model to a realistic time dependent profile for a well depth of 2900 m. The time convention uses zero for the present age and positive numbers for time before present.

Figure 3 contrasts their constant temperature profile to a realistic time dependent one for a well depth of 2900 m. In constructing this time dependent thermal history, I incorporated several major geologic events including the Precambrian uplift of the metamorphic basement, the Paleozoic formation of the Ancestral Rocky Mountains, the gradual burial by Mesozoic sediments, the Laramide orogeny, and recent Quaternary volcanic activity. For those who are interested, a step-by-step construction of the thermal history is given in Appendix A.

As can be seen in Fig. 3, the temperature over the last 500 million years was well below the current temperature. In fact, the volcanic activity which is responsible for the present-day elevated temperatures at the site was so recent that it appears as a vertical spike near zero on the far right-hand side of the figure! By using a constant temperature in their uniformitarian model, the RATE researchers unfairly handicapped the opposing old-earth position. In the language of rhetoric and debate, their tactics would be called a straw man argument.

It is worthwhile, never-the-less, to consider the arguments given by the RATE researchers to justify their constant temperature profile. Their primary sources of information were two thermal modeling studies of the Fenton Hill site, one by Kolstad and McGetchin (1978) and the other by Harrison, Morgan and Blackwell (1986). The RATE team claimed that a constant temperature profile was generous to an uniformitarian model because, according to their

interpretation of these two sources, the temperature was higher at the Fenton Hill site in the past (Humphreys *et al.*, 2003b, p. 184; Humphreys *et al.*, 2004, p. 8; Humphreys, 2005a, pp. 52-55 and 61-62). However, the papers by Kolstad and McGetchin and by Harrison *et al.* both agree that the temperature was actually *lower*, not *higher*, in the past, perhaps even in the recent past.

The following illustration demonstrates the problem with Humphreys' interpretation of these papers. Figure 4 is a reproduction of Kolstad's Figure 11. (Note that Kolstad chose square root time rather than time for the horizontal axis.) A solid horizontal reference line in the lower middle of the figure is drawn at 197 ºC, and corresponds to the current temperature at Fenton Hill at a depth of 2900 m. Consider the model temperature at a similar depth of 3000 m (blue curve) as you read Humphreys' commentary. References are omitted for clarity, emphasis added:

> Our assumption of constant temperatures is generous to the uniformitarian model. Two geoscientists from Los Alamos National Laboratory constructed a theoretical model of the thermal history of the particular borehole (GT-2) we are concerned with. They started by assuming "a background vertical geothermal gradient of 25 ºC/km." … Their model then has an episode of Pliocene-Pleistocene volcanism starting to increase the temperature several megayears ago. It would peak about 0.6 Ma ago at temperatures roughly 50 to 120 ºC above today's values, depending on depth. After the peak, temperatures would decline steadily until 0.1 Ma ago, and then level off at today's values. (Humphreys, 2005a, p. 52)

Although this quotation does describe the shape of the curve we are considering when read from right to left, it is problematic for several reasons. First, the gray band 50 to 120 ºC above the reference line in Fig. 4 represents the interval in which it is claimed that the past temperature reached its peak for a depth of 2900 m. The model temperature at a slightly greater and hotter depth of 3000 m (blue curve) is always below current temperature line and never enters the gray band. This temperature could not have been "50 to 120 ºC above today's values" because it was always numerically *less* than today's value. It is true that the curve has a maximum at 600, drops between 600 and 100, and is mostly level below 100. However, on the left hand side of the figure, the temperature of the blue curve is only 75 ºC, identical to the stated initial condition for a depth of 3000 m in a background geothermal gradient of 25 ºC/km. If zero time corresponds to the initial condition of the theoretical model, then the maximum time must correspond to the final condition (*i.e.* the modern temperature at the site). Therefore, the figure depicts a heating (not cooling) event in which the temperature rises to maximum at a square root time of 600. Humphreys apparently read this figure *backwards*, supposing that time advanced from right to left instead[1].

A similar observation can be made using Harrison's Figure 9, which is reproduced as Fig. 5 in this paper. Again, the horizontal reference line corresponds to the current temperature at a depth of 2900 m. Humphreys' commentary proceeds as follows, emphasis again added:

> Later studies add a more recent pulse of heat and have past temperatures being higher, 110 to 190 ºC more than today's levels just 24,000 years ago, and higher before that. (Humphreys, 2005a, p. 52)

The gray band 110 to 190 ºC above the reference line in Fig. 5 represents the interval in which it is claimed that the past temperature reached its peak for a depth of 2900 m. The model temperature at this same depth (blue curve) is always less than or equal to the current temperature line and never enters the gray band. In no way does this figure depict a temperature that was "110 to 190 ºC more than today's levels". The curve and reference line intersect at only one point, corresponding to a time of 24 ka. Aside from that one point, the model temperature is always below the current temperature. On the left hand side of the figure, the temperature at zero time is only 87 ºC, consistent with the initial condition for a depth of 2900 m in a background geothermal gradient of 30 ºC/km (Harrison *et al.*, 1986). Given these two constraints, the correct interpretation of the figure is that zero time represents the past, and the time of 24 ka represents the present. Once again, it appears that Humphreys read this curve backwards.

Apparently, the temperature values on these curves were never compared against the present-day well temperatures measured at the Fenton Hill site, otherwise this mistake would have been avoided. Perhaps Humphreys assumed that the time axes followed the common geologic convention of using positive numbers to represent time before present. However, thermal modeling would more likely have

[1] It is also possible that Humphreys may have misinterpreted the square root of time scale on the horizontal axis as time in thousands of years.

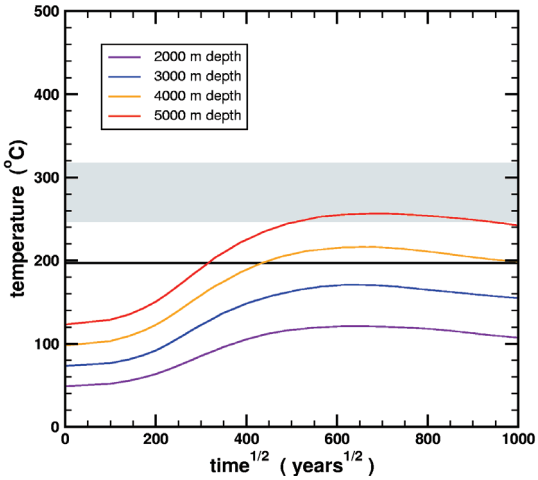

Figure 4. Calculated temperatures at various depths (z) at the location of geothermal test well GT-2 for a pluton of radius 8 km. The solid horizontal reference line at 197 ºC marks the current temperature at Fenton Hill at a depth of 2900 m, and the gray band 50 to 120 ºC above this line represents the interval in which Humphreys claims the past temperature reached its peak for this particular depth. The corresponding model temperature at 3000 m is always less than the current temperature line and never enters the gray band. (Reproduced from Kolstad and McGetchin, 1978, Figure 11. Only the curves for model (a) are shown. Note that the units for the horizontal axis are square root time.)

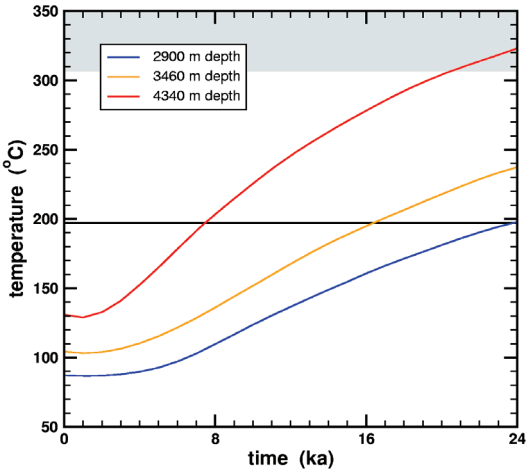

Figure 5. Thermal histories predicted by a 24 ka transient heating event for three different depths. The solid horizontal reference line at 197 ºC marks the current temperature at Fenton Hill at a depth of 2900 m, and the gray band 110 to 190 ºC above this line represents the interval in which Humphreys claims the past temperature reached its peak for this particular depth. The corresponding model temperature at this depth is always less than or equal to the current temperature line and never enters the gray band, part of which lies outside the plot. (Reproduced from Harrison, *et al.*, 1986, Figure 9.)

followed the convention of assigning zero to an event in the past and using positive numbers to represent elapsed model time.

3.5. Material properties

The final error committed by the RATE research team was also the most subtle. The modeling of the helium diffusion clock required an underlying understanding of the diffusion properties of the zircon mineral system. Using data from a laboratory experiment in which gas release from a zircon sample was measured at different temperatures, they extracted the parameters for a simple kinetic model.

The problem with their interpretation of the results from this laboratory experiment is that the few parts per million of gas released at the lowest temperatures (175-255 ºC) were insufficient for constraining the bulk helium diffusion behavior. Here is why. Imagine a regular array of atoms in a crystal with a few isolated defects (Fig. 6). Now place helium atoms randomly throughout this crystal. Most of the helium atoms will lie in portions of the undisturbed crystal lattice (atom **A**), whereas only a small *fraction* will lie in the vicinity of a defect (atom **B**). At low temperatures, the small fraction of atoms near a defect will be mobile (depicted by the bold arrow), whereas the vast majority of atoms will only begin to move at higher temperatures. Essentially, there are two distinct populations of helium atoms in the solid (**A** and **B**), each with different diffusion properties.

This simple example illustrates the concept of a *multi-domain* diffusion model. This type of model has been used by several leading scientists in the noble gas thermochronology field (Reiners and Farley, 1999, pp. 3850-3853; Reiners *et al.*, 2004, pp. 1872-1874; Shuster, *et al.*, 2003, pp. 28-29; Shuster, *et al.*, 2005, pp. 669-670). Instead of using a multi-domain model, the RATE researchers chose a simpler *single-domain* diffusion model, which basically treats all helium atoms as being identical regardless of whether they are located in the bulk lattice or near a defect. Not only did the RATE researchers choose a simplistic kinetic model, but also their lack of discussion of the subject suggests that they were unaware of the existence of alternate models.

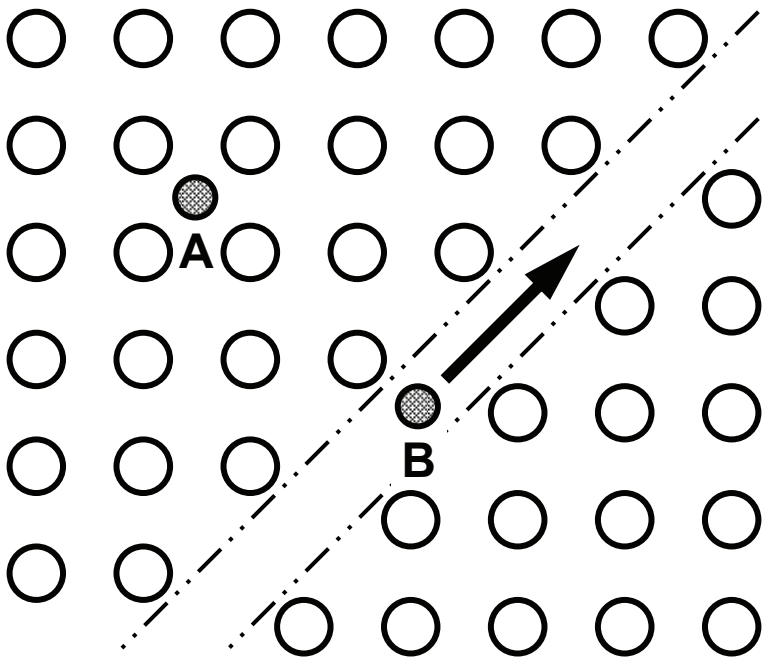

Figure 6. Illustration of a multi-domain diffusion model. The lattice atoms are depicted as large open circles and the helium atoms as small filled circles. The parallel lines represent an extended defect. Helium atom A, which is in a *high retentivity domain* (HRD), is immobile under low temperature diffusion conditions, whereas atom B, which is in a *low retentivity domain* (LRD), is mobile.

Because of the importance of this point, it deserves further elaboration. Several (U-Th)/He thermochronometry studies document complex diffusion behavior. Anomalously high diffusivities were observed in the initial low temperature steps of helium diffusion experiments on titanite (Reiners and Farley, 1999). A multi-domain diffusion mechanism was suggested as a possible explanation for this phenomenon, and synthetic diffusion data for a two-domain model showed the best agreement to measurements when the second domain contained a small fraction of gas and had a much smaller effective radius (and hence higher diffusivity) than the first domain. This second domain was attributed to higher order crystal defects such as microscale cracks and/or irregularities on the surface. In support of this interpretation it was noted that the anomalous diffusion increased for samples which were mechanically abraded. Since only a tiny fraction of gas was attributed to the less retentive domain (less than 1% in some cases), negligible influence was expected on the bulk diffusion and closure temperature of the system, despite the high diffusivity of the secondary domain at low temperatures.

More significantly for the case of Fenton Hill, this same pattern of diffusion was later observed in the helium/zircon system (Reiners *et al.*, 2004). Specifically, anomalously high diffusivities were seen in the early, low temperature stages of a stepwise heating diffusion experiment. This trend was repeatedly observed in many different samples with varying degrees of radioactivity and crystal damage from several different geologic contexts. After considering both U-Th zoning and radiation damage as possible causes for this anomalous behavior, a multi-domain diffusion model was again preferred. When different models were compared with experimental data, the best agreement was consistently found for those cases in which a small fraction of gas in the system (less than 2%) diffused at a much higher rate than the majority of gas (greater by a factor of 40 000 or more). These small gas domains would have little impact on the bulk diffusivity of a zircon crystal (Reiners *et al.*, 2004, pp. 1872-1874). In a summary article on zircon

(U-Th)/He thermochronometry, Reiners made these additional remarks on the subject, emphasis added:

> Zircons with a wide range of ages and radiation dosages exhibited approximately the same degree of non-Arrhenius behavior in initial diffusion steps. Although such modeling does not prove such a mechanism for these non-Arrhenius effects, it suggests that only a small proportion of gas resides in domains that exhibit anomalously high diffusivity, and therefore this phenomenon may not significantly affect the bulk closure temperature or He diffusion properties of most natural zircons. (Reiners, 2005, p. 154)

These findings call into question the validity of the simple helium diffusion model used by the RATE team in their investigation.

Additional evidence can be found in diffusion experiments involving spallogenic ^{3}He released from proton irradiated minerals. These experiments have an advantage over conventional diffusion experiments using natural ^{4}He because after the artificial production of ^{3}He, the samples are kept in a controlled laboratory environment where their thermal histories are precisely known. Consequently, there is an opportunity to probe the kinetics of low retention diffusion domains which might not be detectable in samples that have lost some amount of their natural ^{4}He. When titanite samples from the Fish Canyon tuff were analyzed using this technique, excess ^{3}He and ^{4}He was released during the initial low temperature steps of the experiment (Shuster *et al.*, 2003). The fraction of gas released during these steps was negligible compared to the total (~1% for ^{3}He and 0.5% for ^{4}He). These results corroborate the prior work that was done on the same samples by Reiners and Farley (1999).

Proton irradiation diffusion experiments were subsequently performed on polycrystalline supergene goethite samples (Shuster *et al.*, 2005). Distinct breaks in slope were observed on the ^{3}He Arrhenius plots, and one sample in particular (BAH-F124-111.2) exhibited a clear two slope behavior that is qualitatively similar to what was observed in the Fenton Hill zircons. According to the interpretation of the authors, these features preclude the possibility that a single diffusive length-scale characterizes the helium diffusion in these samples. They go on to say

> The presence of more than a single diffusion domain complicates a diffusion experiment. Gas initially extracted from a distribution of diffusion domains will be a mixture: a larger fraction from less retentive domains and a smaller fraction from more retentive domains. Since the mathematics of Fechtig and Kalbitzer (1966) assume that the gas is derived from a single domain, the presence of a small volume fraction of low retentivity domains will result in values of D/a^2 that are initially higher than the mean for a given temperature. (Shuster *et al.*, 2005, p. 669)

Consequently, the conventional value for diffusivity extracted from a stepwise heating experiment does not adequately describe the true diffusion kinetics of a system if multiple diffusion domains are present. (See Appendix C for an analysis method that can accommodate multiple diffusion domains.)

In order to account for this additional complexity, the gas release from the experiments was studied using a two-domain model (Fig. 6). Helium was partitioned between a *high retentivity domain* (HRD) and a *low retentivity domain* (LRD). In contrast to the work by Reiners *et al.*, who considered multi-domain models in which only the domain radius varied, both the activation energy and domain radius were adjusted by Shuster *et al.* in order to fit the measured data. Consistent with results from prior studies, the best fitting models assigned relatively small gas fractions to the low retentivity domain (4% and 8%) and the remainder to the high retentivity domain. Although these factions were slightly higher than what was previously observed in other mineral systems, this increase is not unreasonable considering the polycrystalline nature of the samples.

In summary, there are several important observations to note regarding these studies. First, anomalously high helium release is frequently observed during the low temperature steps of diffusion experiments involving minerals which are of geologic interest. In particular, zircon is one of these minerals (Reiners *et al.*, 2004; Reiners, 2005). Second, researchers have successfully accounted for this anomalous behavior by using multi-domain diffusion models. A common feature of these models is the partitioning of a small fraction of gas to a low retentivity domain and the remainder to a high retentivity domain. Because of this unequal partitioning, the low retentivity domain has little effect on the bulk helium retention properties of the material over time, despite the domain's higher diffusivity. Finally, the work of these scientists is very relevant to the study at Fenton Hill. Farley, Reiners and Shuster were all members of the same research group that performed the helium diffusion experiments for the RATE team. Ironically, Humphreys and his young-earth colleagues ignored the published works and practices of the same experts whom they contracted to do their laboratory work.

4. A corrected model

4.1. Mathematical framework

The limited modeling framework of the RATE study is inadequate for simulating helium diffusion under the dynamic thermal conditions implied by the complex geologic history of the Fenton Hill site – A more general mathematical algorithm is needed. Meesters and Dunai formulated a diffusion method for (U-Th)/He thermochronology using the eigenfunctions of the Laplacian operator. (Meesters and Dunai, 2002a and 2002b; Dunai, 2005. See Appendix B for a description of this technique.) Their approach has several valuable mathematical features:

1. Arbitrary thermal histories can be modeled.
2. Diffusion and production of helium by radioactive decay are solved simultaneously.
3. Nonhomogeneous radioactive sources can be accommodated.
4. The interaction between diffusion and α-ejection is handled self-consistently.

Several different researchers have applied their method to problems of geologic interest (Lorencak *et al.*, 2004; Persano *et al.*, 2005; Söderlund *et al.*, 2005; Fitzgerald *et al.*, 2006; Kirstein *et al.*, 2006; Foeken *et al.*, 2007; Vermeesch *et al.*, 2007).

The point regarding the interaction between diffusion and α-ejection deserves a brief explanation. There are two primary mechanisms by which helium atoms can leave the zircons. One mechanism is solid-state diffusion. The second mechanism is the immediate ejection of α-particles during radioactive decay, which can account for up to 25-65% of the helium loss for zircons 50-150 μm in length. A correction for this effect was originally performed by the Oak Ridge research team in their calculation of the helium retention ratios (Gentry *et al.*, 1982a). Essentially, the retention values cited were not the ratio of the measured helium to the total helium generated from radioactive decay. Instead, they were the ratio of the measured values to the *fraction* expected to remain after accounting for α-ejection. However, Meesters and Dunai (2002b) pointed out that diffusion and α-ejection are coupled phenomena. Since the α-ejection depletes the helium in the surface region of the crystal, it takes comparatively longer for the remaining helium to escape because it is concentrated toward the center of the crystal. Hence, when the standard correction for α-ejection is made for samples which have also experienced loss due to diffusion, significant errors can result.

4.2. Geometry and boundary conditions

As was previously discussed, a spherical geometry is a reasonably good approximation to a more complex geometry provided that the effective radius is chosen such that the surface-to-volume ratio of the sphere is the same as the real geometry (Meesters *et al.,* 2002a). Accordingly, a sphere with a radius of 20 μm was chosen as the equivalent to tetragonal zircons 50-75 μm in total length. Furthermore, Dirichlet boundary conditions of zero helium concentration at the zircon/biotite interface were used.

Compared to the RATE models, these choices for the geometry and boundary conditions have the effect of accelerating the loss of helium from the crystals, effectively making the diffusion age appear younger. Therefore, one cannot accuse me of being biased in my choice of corrections to the RATE model. As we will see in the simulation results, the impact of using a multi-domain diffusion model along with a geologically derived thermal history more than compensates for these other losses.

4.3. Thermal history

The complex thermal history incorporates several major geologic events including the Precambrian uplift of the metamorphic basement, the Paleozoic formation of the Ancestral Rocky Mountains, the gradual burial by Mesozoic sediments, the Laramide orogeny, and recent Quaternary volcanic activity (Figs. 13 and 14). For those who are interested, a description of the geology of the Fenton Hill site is given in Appendix A.

A starting time of 1440 Ma was chosen for the simulations, based upon the radiometric age of biotite monzogranite dikes (Brookins and Laughlin, 1983). Although gneisses as old as 1620 Ma were found in the Fenton Hill core samples, the heat from the intrusion of the dikes probably would have reset the helium/zircon system. In any event, even the shallowest sample at 750 m was too hot to retain any helium until around 800 Ma (Fig. 10), so the starting time is somewhat arbitrary as long as it is earlier.

4.4. Material properties

The kinetics of the diffusion mechanism was modeled using a multi-domain model. The helium was partitioned between a *high retentivity domain* (HRD) and a *low retentivity domain* (LRD), which were assigned the following diffusion parameters:

$$D_{HRD}(T) = 4.08\times10^{-1}\exp\left(\frac{-38.1\ \text{kcal/mol}}{RT}\right)\ \text{cm}^2/\text{s}$$

$$(\text{gas fraction } 99.7\%), \tag{6}$$

and

$$D_{LRD}(T) = 2.25\times10^{-7}\exp\left(\frac{-13.9\ \text{kcal/mol}}{RT}\right)\ \text{cm}^2/\text{s}$$

$$(\text{gas fraction } 0.3\%). \tag{7}$$

These parameters were extracted from simulations of a stepwise heating experiment. (See Appendix C for details.) The gas fraction in the LRD compares reasonably well with prior estimates of the background helium concentration (Gentry *et al.*, 1982a). The diffusion of gas in the HRD was explicitly modeled in the geologic simulations. The gas in the LRD, on the other hand, was assumed to always be in equilibrium with the background helium concentration of the host rock because of its much higher diffusivity. This small fraction of background gas in the LRD plays an important role in the simulation of the stepwise heating experiment since it is ultimately released in the laboratory under vacuum conditions.

4.5. Radioactive sources

The algorithm of Meesters and Dunai can simultaneously model the diffusion and production of helium by radioactive decay, as well as self-consistently handle the interaction between diffusion and α-ejection. The required inputs are a time-dependent helium source function and a characteristic length for the mean α-particle range.

The time-dependent source function (Fig. 16) included contributions from both uranium and thorium:

$$\begin{aligned} U(t) = {} & 0.83\,U_{decay}(t;\lambda_{238}) \\ & + 0.07\,U_{decay}(t;\lambda_{235}) \\ & + 0.10\,U_{decay}(t;\lambda_{232}), \end{aligned} \tag{8}$$

where the radioactive decay function is given by

$$U_{decay}(t;\lambda) = \frac{\lambda\exp(\lambda t)}{\exp(\lambda t_{\max})-1}, \tag{9}$$

$$t_{\max} = 1440\,\text{Ma},$$

and the specific radioactive decay constants of ^{238}U, ^{235}U, and ^{232}Th are

$$\begin{aligned} \lambda_{238} &= 1.55125\times10^{-10}\ /\ \text{year}, \\ \lambda_{235} &= 9.8485\times10^{-10}\ /\ \text{year}, \\ \lambda_{232} &= 4.9475\times10^{-11}\ /\ \text{year}, \end{aligned} \tag{10}$$

(Steiger and Jäger, 1977). The weights for the three radioactive isotopes are the normalized helium yields expected over 1440 Ma from a radiogenic element concentration of 328.78 ppm uranium and 169.42 ppm thorium (Zartman, 1979). Equations (8)–(9) are normalized so that their integrals are unity over the specified maximum time interval. The time convention uses zero for the present and positive numbers for the past.

In order to determine the mean α-particle range, simulations were performed in which helium accumulated without loss due to diffusion (Fig. 17). When no correction for α-ejection was made in these simulations, the concentration reached unity at the final time as expected (blue curve). When a correction was made using a mean α-particle range of 15.3 μm, the final concentration for a 20 μm sphere dropped to only 45% (orange curve).

This reduction in concentration represents the immediate loss of helium due to α-ejection from the crystal in the absence of any diffusion, and can be compared with a second order polynomial fit to Monte Carlo simulations (Farley, 2002),

$$\begin{aligned} F_T(\beta) = {} & 0.83\,F_{238}(\beta) \\ & + 0.07\,F_{235}(\beta) \\ & + 0.10\,F_{232}(\beta). \end{aligned} \tag{11}$$

Here F_T is the total weighted helium retention fraction and F_{238}, F_{235}, and F_{232} are the specific helium retention fractions for α-particles ejected from ^{238}U, ^{235}U, and ^{232}Th atoms respectively,

$$\begin{aligned} F_{238}(\beta) &= 1 - 4.31\beta + 4.92\beta^2, \\ F_{235}(\beta) &= 1 - 5.00\beta + 6.80\beta^2, \\ F_{232}(\beta) &= 1 - 5.00\beta + 6.80\beta^2. \end{aligned} \tag{12}$$

The parameter β represents the surface-to-volume

ratio of the crystal, which for a 20 μm sphere is equal to

$$\beta = \frac{3}{a} = \frac{3}{20\,\mu\text{m}} = 0.15\,\mu\text{m}^{-1}\,, \tag{13}$$

resulting in helium retention fractions of

$$\begin{aligned} F_{238}(0.15) &= 0.4642 \\ F_{235}(0.15) &= F_{232}(0.15) = 0.4030 \\ F_T(0.15) &= 0.4538\,. \end{aligned} \tag{14}$$

This result agrees well with the numerical simulation. Accordingly, a mean α-particle range of 15.3 μm was used in subsequent simulations, along with Eq. (8) for the time-dependent helium generation rate.

4.6. Numerical implementation

Finally, the time-domain simulations were performed using the eigenfunction method of Meesters and Dunai (2002a and 2002b). A computer program called DECOMP is available from the original authors (Dunai, 2005). However, in order to have better control over the implementation of the algorithm and to support custom features, a computer program was written in the Python scripting language (Beazley, 2000) which included a high performance numerical array extension (Oliphant, 2006; Greenfield *et al.*, 2005). This program was fast enough to handle 10 000 eigenfunctions without a significant time penalty.

For the simulations, a uniform time step of 5 Ma was taken between 1440 Ma and 100 Ma, after which progressively smaller steps were used until a final time of 200 years ago was reached. A total of 826 steps were required for this graded time scale.

5. Results and discussions

In order to better test the accelerated nuclear decay hypothesis, two young-earth models were compared against the corrected model described above, which for the sake of convenience will be called the "old-earth model".

First, the "RATE young-earth model" was constructed to match the published RATE new creation model as closely as possible. It incorporates a 30 μm spherical zircon geometry surrounded by a biotite shell with identical diffusion properties, a constant thermal history, and a single-domain diffusion model simulated over a 6000 year time interval. The only modification made to the original RATE model was the incorporation of the α-ejection effect in the simulations, since the results will be compared against the revised helium retention measurements (Table 1 and Fig. 1) which do not include a correction for α-ejection.

Second, the "revised young-earth model" was constructed to correct the physical geometry and surface boundary condition errors of the original RATE model. It incorporates a smaller 20 μm spherical zircon geometry with a zero helium concentration surface boundary condition. Like the original RATE model, it uses a constant thermal history and a single-domain diffusion model simulated over a 6000 year time interval. Even though it uses a single-domain diffusion model like the RATE model, the kinetic parameters were extracted from simulations of a stepwise heating experiment, as in the old-earth model. (See Appendix C for details.) Therefore, the revised young-earth model corrects most of the RATE errors and is the closest equivalent to the old-earth model. The key differences are its use of a single-domain diffusion model and its young-earth (6000 years) versus old-earth (1.44 billion years) time scale.

A comparison of the results from these three models to measured data is shown in Fig. 7. The old-earth model by far has the best agreement to the revised data. The RATE young-earth model seriously *over-predicts* the helium retention at all depths. However, once the artificial helium retaining effects of the over-sized geometry and zircon/biotite interface conditions are removed, the revised young-earth model seriously *under-predicts* the helium retention. This observation offers a possible insight into why Humphreys might have revised his value for the spherical radius up from his earlier estimate of 22 μm, and why an unrealistic zircon/biotite interface condition was chosen which was not supported by the diffusion data. A realistic young-earth model has serious difficulties matching the measured data without some artificial assistance.

If the reader is perplexed at this point as to how an old-earth model with a 1.44 billion year timescale can show more helium retention than a young-earth model with a 6000 year timescale, the answer is simple: the kinetic model. The old-earth model uses a multi-domain diffusion model whereas the young-earth model, like the RATE study, uses a single-

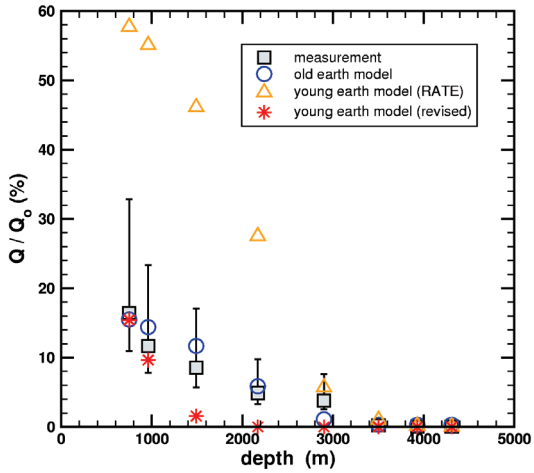

Figure 7. Simulated and measured helium retention ratios versus geothermal well depth. Two young-earth models (triangles and stars) and one old-earth model (circles) are considered. Measured data (squares) are from Table 1.

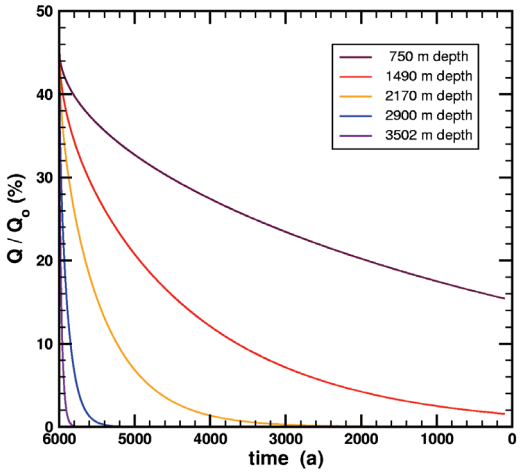

Figure 9. Simulation of the time dependence of the helium retention at five different depths for the revised young-earth model. The time convention uses zero for the present age and positive numbers for time before present.

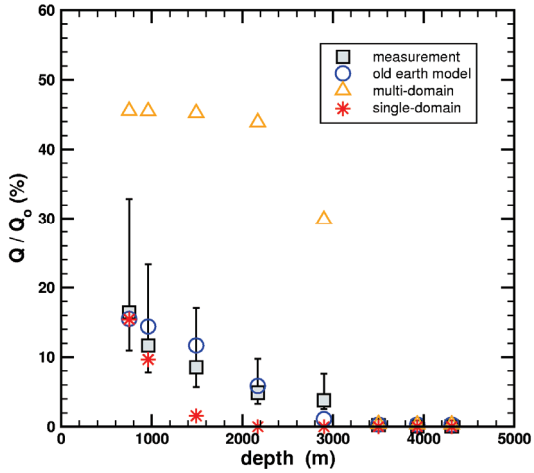

Figure 8. Simulated and measured helium retention ratios versus geothermal well depth. Young-earth models with both single-domain and multi-domain diffusion models are considered. Measured data (squares) are from Table 1.

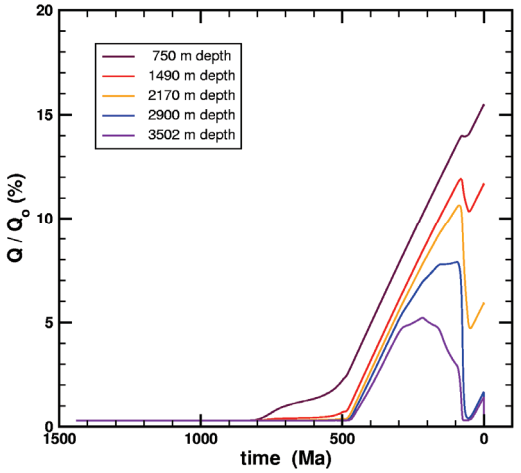

Figure 10. Simulation of the time dependence of the helium growth and retention at five different depths for the old-earth model. The time convention uses zero for the present age and positive numbers for time before present.

domain diffusion model. The difference is that important. It is hard for a realistic single-domain diffusion model to show significant helium retention past a few thousand years. Figure 9 shows the time dependence of the helium retention for the revised young-earth model at five different depths. At a depth of 2900 m, the helium is mostly depleted after only 600 years. At a shallower depth of 2170 m, the helium lasts for about 3000 years. Even at a depth of only 1490 m, most of the helium would be gone in a 6000-year-old earth.

In contrast, Fig. 10 shows the time dependence of the helium retention for the old-earth model. The system at multiple depths closes to helium loss during the Paleozoic, corresponding to a period of uplift which finally brought the Precambrian basement to the surface. Because of continual burial by sediments during the Mesozoic, the system opens

again during the Cretaceous only to have much of these sediments stripped away by the Laramide orogeny. The system again closes to helium loss until the region is heated by recent volcanic activity. At the current temperatures measured down the Fenton Hill wells, the system is again open and slowly losing helium. The zircons below a depth of about 2900 m are now almost completely depleted of their helium content.

If the kinetic model is so important, then what would a young-earth model look like with a multi-domain diffusion model? Figure 8 answers this question. The young-earth model goes from excessive depletion to excessive retention. With the more retentive multi-domain diffusion model, there is now insufficient thermal budget in a young earth to cause *enough* helium loss. The combination that best fits the measured data is a multi-domain diffusion model in the context of an old earth with multiple thermal events occurring over the last 1.44 billion years.

6. Conclusions

Starting with the observed helium retention in zircon crystals from Fenton Hill, the RATE team argued that accelerated nuclear decay had occurred based upon a comparison between two diffusion models constructed according to two different interpretive frameworks. The first model assumed that accelerated nuclear decay had occurred within the last 6000 years, whereas the second model assumed that constant nuclear decay had persisted over a period of 1.5 billion years. Since only their first model succeeded in matching the existing data, the RATE researchers concluded that a young earth with accelerated nuclear decay was the only possible interpretation.

This paper provides an answer to the RATE research at Fenton Hill. Not only does it expose the technical flaws in the RATE study, it also demonstrates that a model consistent with a conventional geologic framework can account for the observed amount of helium contained within these zircon crystals. Accelerated nuclear decay is not required to explain any of the observed phenomena. Rather, through careful attention to details and by applying rigorous mathematical methods, an alternative was found without invoking any exotic physics.

How is the case for accelerated nuclear decay affected by these results? It was claimed that the "diffusion data support the main hypothesis of the RATE research initiative" regarding accelerated nuclear decay (Humphreys *et al.*, 2004, p. 11). What is the logic behind this statement? To put it simply, model **A** (young-earth) worked whereas model **B** (old-earth) failed. Success of the first model alone was insufficient to prove their point, otherwise an investigation of the second model would not have been necessary. The failure of the second model was as vital to the argument as the success of the first model. Without a failed old-earth model, the case for accelerated nuclear decay becomes a circular argument: assume accelerated nuclear decay, match the retention data, and thereby conclude that accelerated decay has occurred. This paper proposes a model that successfully explains the helium retention data within a conventional geologic context. The existence of such a model invalidates the Fenton Hill study of helium diffusion as an argument for accelerated nuclear decay.

The old-earth model matches the revised measurements much better than any of the young-earth models considered. The RATE team claimed that essentially no helium would be left in these zircons if they were much more than a few thousand years old. However, direct computation has demonstrated otherwise – The helium content and the ~1.5 billion year radiometric age of these zircons are in very good agreement. Since no anomaly exists, there is no scientific need to postulate the existence of exotic physics, like accelerated nuclear decay, to explain the phenomenon.

Not only does this result deprive the accelerated nuclear decay hypothesis of its best case, it actually counts as evidence *against* accelerated nuclear decay. Two independent clocks (nuclear decay and helium diffusion) are now in agreement on the billion year age of these rocks. Now the accelerated nuclear decay hypothesis requires accelerated diffusion as well. At some point accelerating natural processes becomes an untenable scientific position, and one must start reading nature's "clocks" at face value.

Appendix A. Geology of the Fenton Hill site

A.1. Location and history

The Fenton Hill site is located on the western margin of the Valles caldera (Fig. 11), a recently active, large resurgent dome volcano. It is part of the larger Jemez Mountains volcanic field (Fig. 12), which is located at the intersection of the north-trending Rio Grande rift and the northeast-trending Jemez volcanic lineament, which encompasses several Miocene to Quaternary volcanic fields (Goff and Gardner, 2004). Geothermal and scientific drilling from 1959 to 1988 produced enormous amounts of information. Fenton Hill, in particular, was the site of four deep geothermal test wells (GT-2, EE-1, EE-2, and EE-3), which ranged in depth from 2930 m to 4390 m, with corresponding bottom hole temperatures ranging from 197 °C (GT-2) to 323 °C (EE-2). Core samples were extracted from all of these wells except EE-3 (Laughlin *et al.*, 1983).

A.2. Radiometric dating

Several different radiometric dating methods have been applied to Precambrian rock samples from the Fenton Hill geothermal wells. Using the Rb-Sr method, an age of 1620 Ma was obtained for 26 gneissic whole rock samples, an age of 1500 Ma was obtained for samples of biotite granodiorite, and an age of 1440 Ma was obtained for samples from dikes of fine-grained biotite monzogranite (Brookins and Laughlin, 1983). K-Ar ages for mica and amphibole range from 1210 Ma to 1440 Ma with a weak depth dependence, and fission track ages of apatite range from zero up to 68.6 Ma with a stronger depth dependence.

All apatite fission track ages are completely reset below a depth of 1880 m (135 ºC current well temperature). The titanite fission track ages, on the other hand, are more commensurate with the K-Ar ages, ranging from 1304 Ma to 1381 Ma, with the exception of one sample from 2900 m which has an age of only 1050 Ma (Brookins *et al.*, 1977). The Rb-Sr dates indicate that the most recent high temperature event was the intrusion of the monzogranite dikes at 1440 Ma. Following this event, it appears that elevated temperatures were sustained for at least another hundred million years or so, based upon the K-Ar dates. A more recent episode of cooling began after 70 Ma, coinciding with the Laramide orogeny.

A.3. Proterozoic to Paleozoic basement exhumation

The metamorphic and structural characteristics of the Precambrian basement exposed throughout northern New Mexico is indicative of a middle-crustal origin from a depth of 10-20 km. Much of this exposed rock stabilized at depths near 10 km and resided there between 1630 and 1480 Ma during the tectonic lull following previous Paleoproterozoic orogenies. The region subsequently experienced Grenville related deformation and plutonism (Karlstrom *et al.*, 2004), and intrusive igneous rock found in the metamorphic basement at Fenton Hill dates from 1500 to 1440 Ma (Brookins and Laughlin, 1983).

The region subsequently experienced exhumation creating the present unconformity between Proterozoic and Mississippian-Pennsylvanian rock (Purtymun *et al.*, 1974; Laughlin *et al.*, 1983; Woodward, 1987, Baltz and Myers, 1999). The critical question is the timing and rate of exhumation between a thermal event at 1440 Ma and the return of a marine depositional environment around 311 Ma.

Harrison *et al.* (1986) noted two distinct features at 870 and 1030 Ma in the $^{40}Ar/^{39}Ar$ age spectra of K-feldspars from Fenton Hill well core samples. Since essentially the same 870 Ma age plateau was observed from three different samples ranging in depth from 1130 to 2900 m, a rapid rate of uplift and erosion was inferred. A similar conclusion was also made regarding $^{40}Ar/^{39}Ar$ age spectra of K-feldspars from the Sangre de Cristo Mountains, which are located approximately 100 km east of the Valles caldera (Sanders *et al.*, 2006). One sample in particular (PVBR01-3) has an age spectrum that is almost identical to the samples of Harrison *et al.* (1986) when it is uniformly shifted down in age by 75 Ma. The thermal model extracted from this sample should be representative of the cooling history of Fenton Hill, provided that it is also shifted by 75 Ma.

The biggest uncertainty in the thermal models extracted by Sanders *et al.* (2006) is the timing of the last 3 to 4 km of basement removal. According to their models, the Precambrian basement was rapidly exhumed from its middle-crustal depth and brought

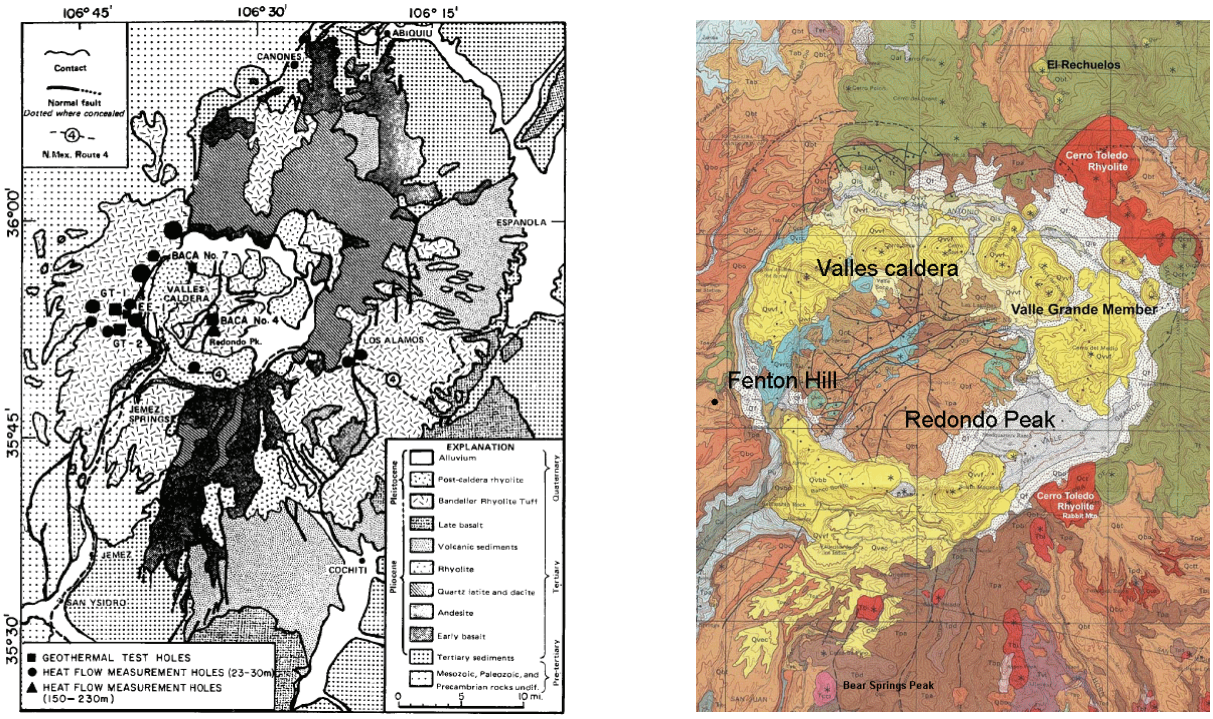

Figure 11. Location and geologic maps of the Valles caldera showing the Fenton Hill well sites (GT-2, EE-1, EE-2, and EE-3). The map on the left is from Kolstad and McGetchin, 1978, Figure 2. The map on the right is from Smith *et al.*, 1970 (annotations added).

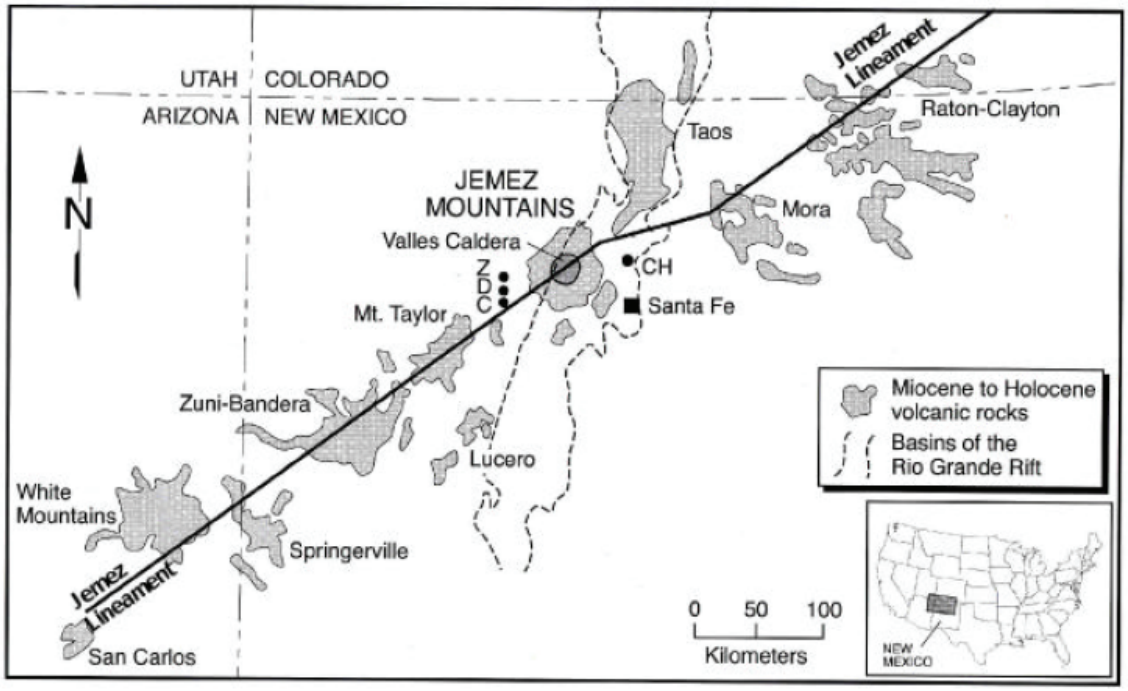

Figure 12. Location map of the Jemez Mountains and Valles caldera with respect to the Jemez volcanic lineament, the Colorado Plateau and the Rio Grande rift (from Goff and Gardner, 2004, Figure 1).

to an upper-crustal environment around 800 to 1000 Ma. The Precambrian rock stabilized at a depth of several kilometers until brought to the surface by a final episode of uplift in the early Paleozoic. The timing of this event is not well constrained by the $^{40}Ar/^{39}Ar$ age data.

Stratigraphic studies provide additional information that can be used to further refine these models. By carefully studying Cambrian and Ordovician sedimentary formations across central Colorado, Myrow *et al.* (2003) concluded that there was no evidence for the highlands of the Transcontinental Arch in southern Colorado and northern New Mexico prior to the Ordovician. Instead, upper Cambrian and lower Ordovician deposits formerly covered a much wider area of these two states than is presently observed. These strata were subsequently removed during an event in the Ordovician approximately 455 Ma called the mid-*Rossodus* uplift.

This uplift correlates with widespread extensional related magmatism throughout New Mexico and Colorado during the Cambrian-Ordovician periods (McMillan and McLemore, 2004). Furthermore, local evidence of this magmatism is found in the southern end of the Sierra Nacimiento approximately 30 km southwest of the Fenton Hill site (Woodward, 1987). By combining these independent lines of evidence, the picture emerges of an episode of extensional related tectonism resulting in regional uplift causing the removal of earlier Paleozoic sedimentary strata and an additional 2 to 4 km of Precambrian crystalline rock.

A.4. Ancestral Rocky Mountains orogeny

Relatively little is know about the geologic history of northern New Mexico from the Ordovician to the Mississippian. Sedimentary rocks of this age are absent from the adjacent Sierra Nacimiento (Woodward, 1987) and the more distant Sangre de Cristo Mountains (Baltz and Myers, 1999). The erosion surface at the base of the Mississippian rocks is relatively flat with little topographical variation (Baltz and Myers, 1999), which is suggestive of a period of slow and gradual erosion without major tectonic disturbance.

By the Mississippian period, the Kaskaskia marine transgression invaded much of the region (Armstrong *et al.*, 2004; Baldridge, 2004). In the Sierra Nacimiento, Mississippian and early Pennsylvanian strata are relatively thin and separated by numerous minor unconformities, indicating that frequent alternation between deposition and erosion occurred.

During the Pennsylvanian period, the Ancestral Rocky Mountains orogeny affected more significant changes to the region. Relative to Fenton Hill, the Taos Trough formed to the east, the San Luis Uplift to the north, and the Peñasco Uplift to the west, the later being the Paleozoic equivalent of the present-day Sierra Nacimiento (Kues and Giles, 2004). The Fenton Hill site itself was in a low-relief shelfal area between mountains and basins. The geothermal test wells penetrated an unconformity separating the Pennsylvanian Sandia Formation from the underlying Proterozoic gneiss at a depth of 730 m (Purtymun *et al.*, 1974; Laughlin *et al.*, 1983).

Uninterrupted marine and terrestrial deposition continued into the Permian comprising the Madera Formation (Pennsylvanian) and Abo Formation (Permian). Later Permian strata are found in the adjacent Sierra Nacimiento (Woodward, 1987), and presumably covered the Fenton Hill site as well until their later removal during the Laramide orogeny.

A.5. Mesozoic sedimentary deposits and the Laramide orogeny

The Triassic and Jurassic strata of northern New Mexico indicate that a net depositional environment prevailed throughout much of the Mesozoic (Lucas, 2004). However, the relative thinness of the corresponding rock units, as compared to the late Paleozoic Madera and Abo Formations, and the existence of numerous unconformities suggest that the depositional processes were less vigorous, with occasional interruptions by periods of erosion (Woodward, 1987).

During the Cretaceous period, the Zuni transgression again flooded the region, returning it to a marine environment (Baldridge, 2004; Nummedal, 2004). Strata of considerable thickness, particularly shales, were deposited at this time (Woodward, 1987). This process ended during the Laramide orogeny, which not only terminated the marine deposition, but also removed the entire column of Mesozoic and upper Paleozoic rock down to the Abo Formation in the vicinity of Fenton Hill (Purtymun *et al.*, 1974; Laughlin *et al.*, 1983; Cather, 2004). Of critical importance is the question of when elevation

of the Fenton Hill site began, because that affects the maximum depth of burial by marine sediments. If uplift began as early as the late Cretaceous, then ~900 m of sediments comprising the Mesaverde group and Lewis shale never covered the site. On the other hand, if uplift began after the Cretaceous, then these strata were deposited and later removed, raising the temperature of the Precambrian basement rock by at least an additional 25 ºC.

Using fission track data from the flanks of the Rio Grande rift, Kelley *et al.* (1992) concluded that the Santa Fe Range, the Los Pinos Mountains, and the eastern margin of the Nacimiento Uplift cooled early during the Laramide orogeny. The Sierra Nacimiento is closest to the Valles caldera and most relevant to our discussion. The exposed Proterozoic rock in the northern part of the mountain range have fission track cooling ages from about 50 to 70 Ma. The mountain range is bounded by faults on the west and gradually slopes down to the east. One sample from the Abo Formation exposed along this eastern margin (88NAC06) had a fission track age as early as 81 Ma. From this result it was inferred that the eastern slope of the Sierra Nacimiento was not deeply buried during the Mesozoic nor strongly uplifted during the early Cenozoic. Significantly, this particular sample (88NAC06) is only 15 km northwest of the Fenton Hill site.

Additional evidence comes from the San Juan basin immediately to the west of the Sierra Nacimiento. Stratigraphic relationships show no sign of differential subsidence prior to ~80 Ma. However, during the Zuni marine transgression, the deposition rate of the Lewis shale doubled to 150 mm/year, and the formation thins both landward and seaward from its point of maximum thickness, indicating that subsidence of the basin had begun prior to the deposition of this formation (Cather, 2004). This event was likely coincident with the uplift of the adjacent Sierra Nacimiento.

Furthermore, in a reconstruction of the exhumation of the Southern Rocky Mountains, Pazzaglia and Kelley (1998) proposed that the northern Sierra Nacimiento is a relatively well preserved Laramide structural feature that has experienced relatively modest erosion rates in the Eocene. Present day erosion rates are higher than both the long term average in the Eocene and the rates of fault offset in the adjacent Rio Grande Rift, suggesting that the currently observed erosion patterns are extremely recent (Formento-Trigilio and Pazzaglia, 1998). These different lines of evidence support a model in which Laramide uplift of the area surrounding the Valles caldera began in the late Cretaceous with subsequent denudation ending by the Oligocene.

A.6. Cenozoic volcanic activity

During the Oligocene, volcaniclastic sediments began to cover the previously exposed erosional surface of the Permian Abo Formation in the vicinity of Fenton Hill (Purtymun *et al.*, 1974; Laughlin *et al.*, 1983; Smith, 2004). Deposition of clastic materials and lava flows from the Jemez volcanic field continued intermittently through the Miocene, culminating in the formation of the Pleistocene Bandelier Tuff during an intense eruptive phase of the Valles caldera (Gardner *et al.*, 1986; Goff and Gardner, 2004). The Bandelier Tuff is the current surface rock layer at the Fenton Hill site.

There are several volcanic events preserved along the southwestern margin of Valles caldera that may have influenced the thermal history of the Fenton Hill site. Earlier eruptions include andesite (8.9 Ma) and dacite (4.0 Ma) lava flows. A small volume of San Diego Canyon tuff (1.8 Ma) erupted from the western side of the site of the modern Valles caldera. The Otowi Member of the Bandelier Tuff was deposited during the eruption and collapse of the Toledo caldera (1.61 Ma), which was subsequently overprinted during the formation of the Valles caldera and the deposition of the Tshirege Member of the Bandelier Tuff (1.25 Ma). There were minor Pleistocene intracaldera eruptions producing rhyolite lava flows and debris deposits. Finally, the youngest volcanic units in the Jemez volcanic field erupted from centers along the southwest ring fracture zone of the Valles caldera, producing the El Cajete Pumice (50-60 ka), the Battleship Rock Tuff (55±6 ka), and the Banco Bonito Rhyolite (40±4 ka). These rock units provide a record of an extremely recent volcanic event (Kelley *et al.*, 2007).

A.7. Thermal modeling

Although the geologic evidence provides excellent chronologic constraints on the thermal history, the temperature constraints must be obtained through other means. Thermally speaking, the most striking feature of the Fenton Hill site is its unusually

high thermal gradient, which is why it has been extensively studied as a potential geothermal energy source.

Kolstad and McGetchin (1978) constructed a theoretical thermal model in which the primary heat source was the emplacement of a cylindrical pluton 8 km in radius at the center of the Valles caldera during a time of high volcanic activity. In their model the temperature rises from a background vertical geothermal gradient of 25 ºC/km to a peak temperature 0.6 Ma ago, after which the temperature remains roughly constant with a slight decline until modern times (Fig. 4). Since the final temperatures predicted by this model were significantly below the ones currently measured down the geothermal test wells, the authors explored another model which assumed the emplacement of a larger pluton 12 km in radius. The predictions of this model matched the current temperatures better, but required that the magma chamber lie directly beneath the GT-2 well at a depth of 3000 m.

Since later deeper wells failed to find any evidence of a recently emplaced pluton (Laughlin *et al.,* 1983), a thermal model postulating a single heating event is probably inadequate for this complex volcanic region. More significantly, geophysical evidence indicates that the size of the pluton emplaced during the eruption of the Valles caldera is much smaller than Kolstad and McGetchin previously envisioned. Bouguer gravity anomaly data outline an elliptically shaped -260 mgal low region, 4 km by 10 km in dimension, centered around the Valles caldera with the long axis trending southwest to northeast (Reiter, 2007). If this gravity anomaly marks the presence of an intrusive thermal source, such as a near-surface granitic body, the horizontal area of this pluton is less than $1/5^{th}$ the size of the pluton assumed in the Kolstad and McGetchin thermal model.

As an alternative, Harrison, Morgan and Blackwell (1986) proposed constraints on the age of heating at Fenton Hill based upon both $^{40}Ar/^{39}Ar$ age spectra for microcline separates and the vertical geothermal gradient. In particular, the curvature of the geothermal gradient could not be adequately explained by variations in the thermal conductivity, which suggests that the basement rock at Fenton Hill is not in thermal steady state. Instead, it is rapidly being heated.

Using this insight, the authors were able to successfully model the modern vertical thermal gradient by assuming a local thermal disturbance 24 ka ago. Starting with a background thermal gradient of 30 ºC/km, the model indicates a sharp and monotonic rise in temperature to its current value over a time span of several thousand years (Fig. 5). Although other thermal models were investigated, the authors noted:

> No reasonable fits to the measured geotherm were obtained for source ages significantly in excess of 40 ka. Thus, if the deep gradient increase in EE-2 is due to conductive heating from a source below Fenton Hill, the source is constrained to be young, much younger than the Valles caldera. (Harrison *et al.*, 1986)

Recent heat sources near the western margin of the Valles caldera appear to be much younger than the main caldera event 1.25 Ma (Reiter, 2007).

One problem with the Harrison model is that a thermal disturbance 24 ka ago does not coincide with any known geologic event. However, in the broader sense, the main point of their work is that a recent geologic event is responsible for the elevated thermal gradient presently observed at the Fenton Hill site. Given the uncertainty inherent in their model, the eruption at El Cajete crater around 50 ka cannot be ruled out as the source event. There are several lines of reasoning favoring this correlation. First, a volcanic eruption at 50 ka roughly fits within the upper time limit of 40 ka for the source age (Harrison *et al.*, 1986). Second, these eruptions were along the southwest margin of the Valles caldera, which is close to the Fenton Hill site. Third, the curvature in the geothermal gradient, noted by Harrison *et al.*, is a hard geophysical constraint limiting the age of the source event. Finally, test well and gravity anomaly data disfavor the Kolstad and McGetchin thermal model, which attempted to ascribe the heating to an earlier eruption of the Valles caldera around 1.25 Ma.

A.8. Summary

The events of the foregoing geologic history are summarized in Table 2. The thicknesses of strata preserved at the site are directly known from well data (Purtymun *et al.*, 1974). For strata inferred to have been present at one time and subsequently removed by erosion, thicknesses were estimated from a detailed geologic study of the vicinity (Woodward, 1987). In cases where a range of thicknesses was reported for a given rock unit, the median value was used. Most unconformities in the stratigraphic history were treated as periods during which neither

deposition nor erosion occurred, although the possibility of an episode of deposition followed by subsequent erosion is certainly possible. The thermal contribution from such events is expected to be relatively minor, however.

Two major periods of erosion are recognized, one during the Ordovician (mid-*Rossodus* uplift) and the other from the Cretaceous to the Oligocene (Laramide orogeny). A third period is possible during the incipient phase of the Ancestral Rocky Mountains orogeny. However, the presence of the Pennsylvanian Sandia Formation above the Precambrian surface limits the duration of any possible episode of erosion.

The time of the different events in Table 2 are drawn from a variety of sources, as indicated in the table caption. Two references deserve special attention. First, the late Proterozoic cooling history was taken from the $^{40}Ar/^{39}Ar$ dating work of Sanders *et al.* (2006). The monotonic thermal model for sample PVBR01-3 was shifted down in age by 75 Ma and used to represent the temperature at a depth of 730 m, which is the upper surface of the Precambrian basement rock. Second, the cooling history during the Laramide orogeny was taken from the fission track studies of Kelley *et al.* (1992). The thermal model for the northern block of the Sierra Nacimiento (sample 88NAC09) was proportionally scaled to match the corresponding thickness of Mesozoic and Paleozoic strata expected to have been removed by erosion during uplift of the area.

The thermal history of the Fenton Hill site for different present-day depths was calculated from this stratigraphic history by assuming a thermal gradient of 25 ºC/km and a surface temperature of 12 ºC. This approach was used up until the Pleistocene, when volcanic eruptions in the Jemez Mountains began to dominate the thermal landscape.

Starting in the Pleistocene, the thermal history was constructed from modified versions of the thermal models of Kolstad and McGetchin (1978) and Harrison, Morgan and Blackwell (1986). The Kolstad and McGetchin model was adjusted both in time and temperature. The beginning of the heating episode was shifted to 1.25 Ma to coincide with the eruption of the Valles caldera (Kelley *et al.*, 2007), and the magnitude of the event was scaled to match the area of the pluton inferred from gravity anomaly data (Reiter, 2007). The temperature adjustment, in particular, had the effect of significantly reducing the impact which the 1.25 Ma eruption of the Valles caldera had on the current well temperatures at the Fenton Hill site. Consistent with the Harrison model, a significant portion of the heating occurs within the last 50 000 years. Their model was adjusted in time to 50 ka so that the beginning of the heating event would coincide with the eruptions at El Cajete crater (Kelley *et al.*, 2007). The thermal history of Fenton Hill at several depths is plotted on both a linear (Fig. 13) and logarithmic (Fig. 14) time axis.

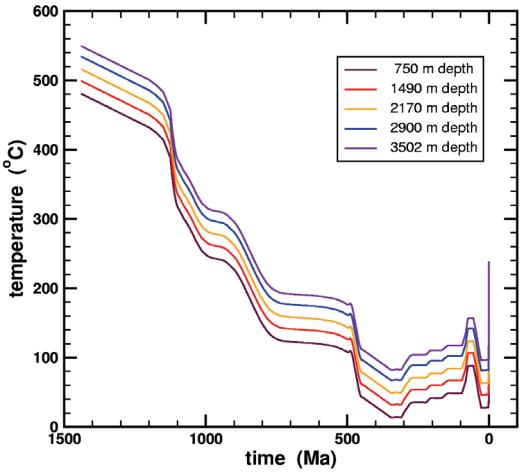

Figure 13. The thermal history of the Fenton Hill site at five selected depths plotted on a linear time axis. The time convention uses zero for the present age and positive numbers for time before present.

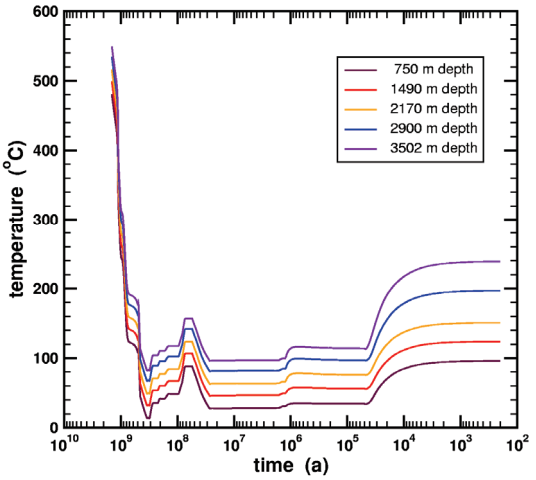

Figure 14. The thermal history of the Fenton Hill site at five selected depths plotted on a logarithmic time axis. The time convention uses zero for the present age and positive numbers for time before present.

Table 2
Deposition and erosion events affecting the thermal history of Fenton Hill, NM. The depth is referenced with respect to the present-day surface, with positive numbers indicating overlying rock units which are no longer present in the column and negative numbers indicating the absence of current rock units in the past. The times designate the end of a given deposition or erosion event. The geologic history was constructed using the following sources:

(1) K-feldspar $^{40}Ar/^{39}Ar$ age spectra, southern Sangre de Cristo Range, NM (Sanders *et al.*, 2006).
(2) K-feldspar $^{40}Ar/^{39}Ar$ age spectra, Fenton Hill, NM (Harrison *et al.*, 1986).
(3) stratigraphy, central Colorado (Myrow *et al.*, 2003).
(4) igneous intrusions, Colorado and New Mexico (McMillan and McLemore, 2004).
(5) well core data, Fenton Hill, NM (Purtymun *et al.*, 1974).
(6) stratigraphy, Sierra Nacimiento, NM (Woodward, 1987).
(7) apatite fission-track dating, Sierra Nacimiento, NM (Kelley *et al.*, 1992).
(8) radiometric dating, Jemez Volcanic Field, NM (Gardner *et al.*, 1986).
(9) stratigraphy, Sierra Nacimiento, NM (Armstrong *et al.*, 2004).
(10) stratigraphy, Sierra Nacimiento, NM (Kues and Giles, 2004).
(11) stratigraphy, north-central New Mexico (Lucas, 2004).
(12) stratigraphy, San Juan Basin, NM (Nummedal, 2004).
(13) stratigraphy, San Juan Basin and Sierra Nacimiento, NM (Cather, 2004).
(14) stratigraphy, Rio Grande Rift, NM (Smith, 2004).
(15) radiometric dating, Jemez Volcanic Field, NM (Goff and Gardner, 2004).

Time (Ma)	Duration (Ma)	Depth (km)	Change (km)	Period or Epoch	Description
500		3.080		Cambrian	initial depth [1, 2]
485	15	3.130	0.050	Cambrian	various formations [3]
455	30	0.580	-2.550	Ordovician	mid-Rossodus uplift [3] (widespread extensional related magmatism) [4, 6]
345	110	-0.700	-1.280	Ordovician to Mississippian	gradual erosion assumed
320	25	-0.650	0.050	Mississippian	various formations [6, 9]
311	9	-0.730	-0.080	Pennsylvanian	Penasco uplift [5, 6, 10] (Ancestral Rocky Mountains orogeny)
308	3	-0.650	0.080	Pennsylvanian	Sandia Formation [5, 6, 10]
299	9	-0.375	0.275	Pennsylvanian	Madera Formation [5, 6, 10]
280	19	0.075	0.450	Permian	Abo Formation [5, 6, 10]
275	5	0.155	0.080	Permian	Yeso Formation [6, 10]
270	5	0.175	0.020	Permian	Glorieta Sandstone [6, 10]
265	5	0.185	0.010	Permian	Bernal Formation [6]
220	45	0.185	0.000	Permian to Triassic	unconformity [6, 11]
208	12	0.435	0.250	Triassic	Chinle Formation [6, 11]
164	44	0.435	0.000	Triassic to Jurassic	unconformity [6, 11]
162	2	0.495	0.060	Jurassic	Entrada Sandstone [6, 11]
161	1	0.515	0.020	Jurassic	Todilto Formation [6, 11]
145	16	0.715	0.200	Jurassic	Morrison Formation [6, 11]
95	50	0.715	0.000	Jurassic to Cretaceous	unconformity [6, 12]
94	1	0.765	0.050	Cretaceous	Dakota Formation [6, 12]
82	12	1.405	0.640	Cretaceous	Mancos Shale [6, 12]
79	3	1.745	0.340	Cretaceous	Mesaverde Group [6, 12]
74	5	2.295	0.550	Cretaceous	Lewis Shale [6, 12]
27	47	-0.135	-2.430	Cretaceous to Oligocene	Laramide orogeny [5, 6, 7, 13] (including subsequent rift related uplift)
25.1	1.9	-0.120	0.015	Oligocene	Abiquiu Tuff [5, 6, 14]
10.6	14.5	-0.120	0.000	Oligocene to Miocene	hiatus [5, 6, 14]
8.69	1.91	-0.105	0.015	Miocene	Paliza Canyon Formation [5, 6, 14]
1.64	7.05	-0.105	0.000	Miocene to Pleistocene	hiatus [5, 6, 14]
1.57	0.07	-0.075	0.030	Pleistocene	Bandelier Tuff [5, 6, 8, 15] (Otowi Member)
1.22	0.35	-0.075	0.000	Pleistocene	hiatus [5, 6, 8, 15]
1.19	0.03	0	0.075	Pleistocene	Bandelier Tuff [5, 6, 8, 15] (Tshirege Member)

Appendix B. Mathematics of the diffusion method

B.1. Theoretical foundation

The development of the diffusion method in this section closely follows Appendix A of Meesters and Dunai (2002a, pp. 341-343) until Eq. (28), after which an alternate approach is pursued. A computer program called DECOMP is available from the original authors (Dunai, 2005). The starting point in the derivation of the method is the diffusion equation including a source term,

$$\frac{\partial C}{\partial t} = D(t)\nabla^2 C + S(x,y,z)U(t). \tag{15}$$

In this partial differential equation, C is the space and time dependent concentration of the diffusing species, D is a possibly time dependent diffusion coefficient, S is the space dependent source distribution, and U is the time dependent source rate. It is assumed that the source term can be separated into a product of a space dependent function S and a time dependent function U. This assumption is reasonable since in the case of helium diffusion, the source is the radioactive elements in the crystal, whose positions are fixed at the time of crystallization. The rate of helium generation, however, may not be constant with time.

The diffusion equation cannot be solved analytically for the general case of an arbitrary geometry, diffusion coefficient, source term, and boundary condition. Therefore, a numerical alternative must be sought. Following the approach of Meesters and Dunai, the diffusion equation is reformulated using the eigenfunctions of the Laplacian operator:

$$\nabla^2 u_n = -\mu_n u_n . \tag{16}$$

These eigenfunctions must satisfy the boundary condition for the geometry under consideration. Once determined, the concentration of the diffusing species can be expressed as

$$C(x,y,z,t) = \sum_{n=1}^{\infty} f_n(t)\, u_n(x,y,z), \tag{17}$$

with the spatial part of the source function expanded as

$$S(x,y,z) = \sum_{n=1}^{\infty} s_n\, u_n(x,y,z). \tag{18}$$

When these two series are substituted into Eq. (15), the partial differential equation decomposes into a series of ordinary time-dependent differential equations:

$$\frac{df_n(t)}{dt} = -\mu_n\, D(t) f_n(t) + s_n\, U(t). \tag{19}$$

The solution of these equations gives the coefficients to the eigenfunctions in the series expansion of Eq. (17). If only the average concentration is desired and not the spatial details of the profile, a further simplification can be made by taking the spatial average of Eq. (19) weighted by each corresponding eigenfunction. The result can be expressed as

$$\frac{dc_n(t)}{dt} = -\mu_n\, D(t) c_n(t) + \gamma_n\, U(t), \tag{20}$$

where the average concentration and source terms are written using the spatially averaged eigenfunctions as

$$c_n(t) = f_n(t)\,\overline{u}_n , \tag{21}$$

and

$$\gamma_n = s_n\,\overline{u}_n . \tag{22}$$

The average of an eigenfunction is defined as its volume integral averaged over the diffusion domain,

$$\overline{u}_n = \frac{\int u_n(x,y,z)\,dV}{V}. \tag{23}$$

Furthermore, the source coefficients can be determined by projecting the source function onto the basis of eigenfunctions,

$$s_n = \frac{\int S(x,y,z)\, u_n(x,y,z)\,dV}{\int u_n{}^2(x,y,z)\,dV}, \tag{24}$$

provided that the basis functions are orthogonal. Using these definitions, Eq. (17) simplifies to

$$\begin{aligned}\overline{C}(t) &= \frac{\int C(x,y,z,t)\,dV}{V} \\ &= \sum_{n=1}^{\infty} f_n(t)\,\overline{u}_n = \sum_{n=1}^{\infty} c_n(t),\end{aligned} \tag{25}$$

when averaged over the diffusion domain.

Once these expansions and substitutions are made, the exact solution to the diffusion equation can be formally expressed as a sum of time dependent concentration functions:

$$c_n(t) = c_n(t_o)\exp\left(-\mu_n \xi(t)\right) + \gamma_n\, G_n(t). \tag{26}$$

Here

$$\xi(t) = \int_{t_o}^{t} D(\theta)\, d\theta\,, \tag{27}$$

and

$$G_n(t) = \int_{t_o}^{t} U(\theta)\exp\left(-\mu_n\left(\xi(t) - \xi(\theta)\right)\right) d\theta\,. \tag{28}$$

In principle, Eq. (26) is exact since no approximations have been made to this point. However, the solution as it stands is not practical because of the double integration implied by Eqs. (27)–(28). To arrive at a more computationally tractable method, some simplifications must be made. Meesters and Dunai proceeded by making a variable transformation along with further approximations (Meesters and Dunai, 2002a). After considering their approach, it was felt that an alternate formulation was preferable.

First, noting that at some point discretization of time would probably be needed in order to handle arbitrary diffusion and source histories, Eq. (26) was recast as a recursion formula in which the solution at a subsequent time step is given in terms of the variables at the current time step:

$$c_n(t_{k+1}) = c_n(t_k)\exp\left(-\mu_n \xi(t_{k+1})\right) + \gamma_n\, G_n(t_{k+1}). \tag{29}$$

Here

$$\xi(t_{k+1}) = \int_{t_k}^{t_{k+1}} D(\theta)\, d\theta\,, \tag{30}$$

and

$$G_n(t_{k+1}) = \int_{t_k}^{t_{k+1}} U(\theta)\exp\left(-\mu_n\left(\xi(t_{k+1}) - \xi(\theta)\right)\right) d\theta\,. \tag{31}$$

Since the choice of time step is arbitrary, it can be selected such that the time dependent diffusion coefficient D and source rate U are approximately constant over each time interval.[2] Once this simplification is made, the time dependent variables can be taken outside the integrals leaving just

$$\begin{aligned}\xi(t_{k+1}) &= D_{k+1}\int_{t_k}^{t_{k+1}} d\theta \\ &= D_{k+1}\left(t_{k+1} - t_k\right) = D_{k+1}\,\Delta t_{k+1}\,,\end{aligned} \tag{32}$$

and

$$\begin{aligned}G_n(t_{k+1}) &= U_{k+1}\int_{t_k}^{t_{k+1}} \exp\left(-\mu_n D_{k+1}\left(t_{k+1} - \theta\right)\right) d\theta \\ &= U_{k+1}\left(\frac{1 - \exp\left(-\mu_n D_{k+1}\left(t_{k+1} - t_k\right)\right)}{\mu_n D_{k+1}}\right) \\ &= U_{k+1}\,\Delta t_{k+1}\left(\frac{1 - \exp\left(-\mu_n D_{k+1}\,\Delta t_{k+1}\right)}{\mu_n D_{k+1}\,\Delta t_{k+1}}\right).\end{aligned} \tag{33}$$

If the modified exponential function is used,

$$\exp 1(x) = \frac{\exp(x) - 1}{x} = \sum_{p=0}^{\infty} \frac{x^p}{(p+1)!}\,, \tag{34}$$

the final recursion formula for the concentration functions becomes

$$c_n(t_{k+1}) = c_n(t_k)\exp\left(-A_{n,k+1}\right) + B_{n,k+1}\,\exp 1\left(-A_{n,k+1}\right), \tag{35}$$

where

$$A_{n,k+1} = \mu_n\, D_{k+1}\,\Delta t_{k+1}\,, \tag{36}$$

and

$$B_{n,k+1} = \gamma_n\, U_{k+1}\,\Delta t_{k+1}\,. \tag{37}$$

This elegant result is quite general, intuitively appealing, numerically robust, and computationally efficient. It is quite general because provided that the time step is suitably chosen and sufficiently small, arbitrary temperature histories and source functions can be accommodated. It is intuitively appealing because the diffusivity and the source function appear in the formula as simple products with the time step. It is numerically robust because it can readily handle discontinuities in D and U provided that time steps are chosen at these points. In fact, the assumptions of the method become better fulfilled at a discontinuity, and it is ideally suited for simulating a stepwise heating diffusion experiment. Finally, it is computationally efficient. Time steps are required only when the diffusion coefficient or source function is changing significantly. No method error is incurred if a long time step is taken during an interval in which these variables are constant.

[2] This type of approximation is similar to that used in first order numerical integration methods.

The space dependent quantities μ and γ can be calculated once for a given geometry independent of the diffusion and source histories. The time dependent quantities *D* and *U*, on the other hand, can be discretized and multiplied by the time step independent of the geometry. Once calculated and stored, these quantities can be readily multiplied together when the recursion algorithm begins. If the programming language used for simulation supports vector arithmetic, the algorithm can be made extremely efficient.

To estimate the amount of computation required, if *N* eigenfunctions are used with *M* time steps, the total number of mathematical operations will be on the order of *MN*. As a concrete example, if 10 000 eigenfunctions are used with 100 time steps, on the order of 1 000 000 operations will be required, a rather modest number considering the speed of modern desktop computers. One final comment should be made regarding numerical computation. In the very realistic case of high retention and low diffusivity, direct computation of the modified exponential function in Eq. (34) using analytic functions can have high cancellation errors. Under these circumstances, the series expansion, which converges quite rapidly under these circumstances, is preferred.

B.2. Specific applications

Before proceeding with the application of the diffusion method to specific geometries and boundary conditions, it is helpful to first define some basic integrals involving trigonometric functions:

$$\mathrm{I}_0(r;k_n)=\int \sin(k_n r)\,dr=\frac{-\cos(k_n r)}{k_n}, \tag{38}$$

$$\mathrm{I}_1(r;k_n)=\int \sin(k_n r)\,r\,dr=\frac{-(k_n r)\cos(k_n r)+\sin(k_n r)}{k_n^2}, \tag{39}$$

$$\mathrm{I}_2(r;k_n)=\int \sin(k_n r)\,r^2\,dr=\frac{-(k_n r)^2\cos(k_n r)+2(k_n r)\sin(k_n r)+2\cos(k_n r)}{k_n^3}, \tag{40}$$

$$\mathrm{I}_S(r;k_n)=\int \sin^2(k_n r)\,dr=\frac{1}{2}\left(r-\frac{\sin(2k_n r)}{2k_n}\right), \tag{41}$$

$$\mathrm{I}_X(r;k_1,k_2)=\int \sin(k_1 r)\sin(k_2 r)\,dr=\frac{1}{2}\left(\frac{\sin(k_d r)}{k_d}-\frac{\sin(k_s r)}{k_s}\right), \tag{42}$$

where

$$k_1\neq k_2\ ,\quad k_s=k_1+k_2\ ,\quad k_d=k_1-k_2\ . \tag{43}$$

For a diffusion problem with spherical symmetry, the radial functions

$$u_n(r)=\frac{1}{r}\sin(k_n r), \tag{44}$$

are eigenfunctions of the Laplacian operator,

$$\nabla^2 u_n=-\mu_n u_n\ =-k_n^2\,u_n\ , \tag{45}$$

and, unlike the complementary cosine solution, are also nonsingular at the origin. The eigenvalues for a Dirichlet boundary condition of zero on a sphere of radius *a* are

$$k_n=\frac{n\pi}{a}, \quad \text{if } \sin(k_n a)=0 \text{ and } \cos(k_n a)=(-1)^n\ . \tag{46}$$

Dirichlet boundary conditions with a nonzero concentration can also be accommodated. In this case the solution represents the concentration in excess of the boundary value. The spatial average of these eigenfunctions and their normalization integrals can be directly calculated as

$$\bar{u}_n = \frac{4\pi}{V}\int_0^a u_n(r) r^2 dr = \frac{4\pi}{V}\int_0^a \sin(k_n r) r\, dr$$
$$= \frac{3}{a^3}\,\mathrm{I}_1(a;k_n) = \frac{(-1)^{n+1}3}{(n\pi)a}, \tag{47}$$

and

$$4\pi\int_0^a u_n^2(r) r^2 dr = 4\pi\int_0^a \sin^2(k_n r) dr$$
$$= 4\pi\,\mathrm{I}_S(a;k_n) \tag{48}$$
$$= 4\pi\left(\frac{a}{2}\right).$$

The final expressions in Eqs. (47)–(48) were obtained by substituting the eigenvalues from Eq. (46) into the trigonometric integrals which were previously defined. This substitution is valid only if Dirichlet boundary conditions apply. For other boundary conditions, such as Neumann or mixed boundaries, the more general integral expressions must be used instead. Although realistic problems of interest such as helium diffusion in zircon crystals rarely have ideal spherical symmetry, to good approximation a sphere can be used to model a more complex geometry provided that both systems have the same surface-to-volume ratio (Meesters and Dunai, 2002a, pp. 340-341).

Once the eigenfunctions are known, the coefficients for the series expansion of the source function can be determined. The simplest example to consider is a uniform radioactive source with no correction for α-ejection. In this case, the radial source function is given by

$$S(r) = 1. \tag{49}$$

The relevant integrals and coefficients can be directly calculated as

$$4\pi\int_0^a S(r) u_n(r) r^2 dr = 4\pi\int_0^a \sin(k_n r) r\, dr$$
$$= 4\pi\,\mathrm{I}_1(a;k_n) \tag{50}$$
$$= 4\pi\left(\frac{(-1)^{n+1}(n\pi)}{k_n^2}\right),$$

$$s_n = \left(\frac{2}{a}\right)\left(\frac{(-1)^{n+1}(n\pi)}{k_n^2}\right) = \frac{(-1)^{n+1}2}{k_n}, \tag{51}$$

$$\gamma_n = \left(\frac{(-1)^{n+1}2}{k_n}\right)\left(\frac{(-1)^{n+1}3}{(n\pi)a}\right) = \frac{6}{(n\pi)^2}. \tag{52}$$

Once again these equations are valid only for Dirichlet boundary conditions.

If a correction for α-ejection is made, several possibilities must be considered depending upon the relationship between the mean α-particle range σ and the radius of the sphere *a*. If

$$\sigma < a, \tag{53}$$

the radial source function is given by

$$S(r;\sigma) = \begin{cases} 1 & \text{if } \mathbf{A} \\ \left(a^2 - (r-\sigma)^2\right)/(4\sigma r) & \text{if } \mathbf{B} \end{cases}, \tag{54}$$

where

$$\begin{aligned} &\mathbf{A}: \quad r \le a - \sigma \\ &\mathbf{B}: \quad a - \sigma \le r \le a + \sigma, \end{aligned} \tag{55}$$

(Meesters and Dunai, 2002b, p. 353). The resulting equation for the source integral is more involved but still tractable,

---

$$4\pi\int_0^a S(r;\sigma) u_n(r) r^2 dr = 4\pi\int_0^{a-\sigma} \sin(k_n r) r\, dr + \frac{\pi}{\sigma}\int_{a-\sigma}^a \left(a^2 - \sigma^2 + 2\sigma r - r^2\right)\sin(k_n r) dr$$
$$= 4\pi\int_0^a \sin(k_n r) r\, dr + \frac{\pi}{\sigma}\int_{a-\sigma}^a \left(a^2 - \sigma^2 - 2\sigma r - r^2\right)\sin(k_n r) dr \tag{56}$$
$$= 4\pi\left(\mathrm{I}_1(a;k_n) + \frac{1}{4\sigma}\left[\mathrm{I}_\alpha(a;k_n,a,\sigma) - \mathrm{I}_\alpha(a-\sigma;k_n,a,\sigma)\right]\right),$$

where

$$\mathrm{I}_\alpha(r;k_n,a,\sigma)=\left(a^2-\sigma^2\right)\mathrm{I}_0(r;k_n)-2\sigma\,\mathrm{I}_1(r;k_n)-\mathrm{I}_2(r;k_n). \tag{57}$$

The similarity between Eqs. (50) and (56) should be noted, with the latter containing an additional term representing the α-ejection correction. If Dirichlet boundary conditions are again assumed, the resulting source coefficients reduce to

$$s_n=\left(\frac{(-1)^{n+1}}{k_n}\right)\left(1-\frac{\sigma}{2a}+\frac{1}{n\pi}\frac{1}{k_n\sigma}\left(1-\cos(k_n\sigma)\right)+\frac{1}{k_n\sigma}\sin(k_n\sigma)\right), \tag{58}$$

$$\gamma_n=\left(\frac{3}{(n\pi)^2}\right)\left(1-\frac{\sigma}{2a}+\frac{1}{n\pi}\frac{1}{k_n\sigma}\left(1-\cos(k_n\sigma)\right)+\frac{1}{k_n\sigma}\sin(k_n\sigma)\right). \tag{59}$$

Derivation of Eqs. (58)–(59) from Eqs. (56)–(57) is straight forward but tedious, and is omitted here for simplicity. However, it should be noted that Eq. (59) agrees with prior work (Meesters and Dunai, 2002b, p. 353, Equation 24).

The last case of interest discussed by Meesters and Dunai is a radial zoned source with a correction for α-ejection (Meesters and Dunai, 2002b, pp. 353-354). If

$$\sigma<a;\quad z_2\le a-\sigma;\quad z_1<z_2, \tag{60}$$

where σ is the mean α-particle range, z_1 is inner radius of the zone, and z_2 is the outer radius of the zone, then

$$4\pi\int_0^a S(r;z_1,z_2,\sigma)u_n(r)r^2dr=4\pi\left(\frac{\sin(k_n\sigma)}{k_n\sigma}\left[\mathrm{I}_1(z_2;k_n)-\mathrm{I}_1(z_1;k_n)\right]\right). \tag{61}$$

and the source coefficients are

$$s_n=\left(\frac{2}{a}\right)\left(\frac{\sin(k_n\sigma)}{k_n\sigma}\left[\mathrm{I}_1(z_2;k_n)-\mathrm{I}_1(z_1;k_n)\right]\right), \tag{62}$$

$$\gamma_n=\left(\frac{(-1)^{n+1}6}{(n\pi)a^2}\right)\left(\frac{\sin(k_n\sigma)}{k_n\sigma}\left[\mathrm{I}_1(z_2;k_n)-\mathrm{I}_1(z_1;k_n)\right]\right). \tag{63}$$

The significance of this zoned model is that it can be used to represent the creation model of Humphreys. In his model, a zircon sphere of radius *a* was embedded in a biotite sphere of radius *b*. Since the diffusivities of the two materials were taken to be equal, there was essentially no difference between zircon and biotite. Therefore, the model can be equivalently formulated as a large sphere of zircon with a radial zoned radioactive source in which

$$a\to b;\quad z_1\to 0;\quad z_2\to a. \tag{64}$$

In this case the eigenvalues are determined by the radius of the large "biotite" sphere,

$$k_n=\frac{n\pi}{b}. \tag{65}$$

The subtlety, however, is that the spatial average of the eigenfunctions must be made over the small *inner* sphere, not the large *outer* sphere,

$$\begin{aligned}\bar{u}_n &= \frac{4\pi}{V}\int_0^a u_n(r)r^2\,dr = \frac{4\pi}{V}\int_0^a \sin(k_n r)r\,dr \\ &= \frac{3}{a^3}\,\mathrm{I}_1(a;k_n).\end{aligned} \tag{66}$$

The reason for this unconventional definition of the spatial average is that we are interested in the amount of helium retained in the inner "zircon" sphere, not the outer "biotite" sphere. Once this definition is made, the corresponding source coefficients are

$$s_n = \left(\frac{2}{b}\right)\left(\frac{\sin(k_n\sigma)}{k_n\sigma}\,\mathrm{I}_1(a;k_n)\right), \tag{67}$$

$$\gamma_n = \left(\frac{6}{a^3 b}\right)\left(\frac{\sin(k_n\sigma)}{k_n\sigma}\,\mathrm{I}_1^2(a;k_n)\right). \tag{68}$$

This model is similar to the creation model of Humphreys except for the additional correction for α-particle ejection.

Mathematical equivalence with the original formulation of Humphreys' creation model can be demonstrated (Humphreys, 2005a, pp. 46-51). The α-particle correction is removed by taking the limit as the mean range goes to zero. The initial concentration is generated by a unit pulse of radioactive decay at time zero,

$$c_n(0) = \gamma_n\,. \tag{69}$$

The final concentration for each eigenfunction is calculated using a single time step in Eq. (35), since constant temperature is assumed for the duration of the simulation,

$$c_n(t) = c_n(0)\exp(-\mu_n\,Dt\,). \tag{70}$$

Here the source term is set to zero because all the radioactive decay is assumed to have occurred during the initial pulse. The final concentration is simply the sum of all the individual eigenfunction contributions,

$$\overline{C}(t) = \sum_{n=1}^{\infty} c_n(t) = \sum_{n=1}^{\infty}\gamma_n\exp\left(-\frac{(n\pi)^2\,Dt}{b^2}\right), \tag{71}$$

$$\begin{aligned}\gamma_n &= \left(\frac{6}{a^3 b}\right)\mathrm{I}_1^2(a;k_n) = \left(\frac{6b^3}{(n\pi)^4 a^3}\right) \\ &\times\left(\left(\frac{n\pi a}{b}\right)\cos\left(\frac{n\pi a}{b}\right) - \sin\left(\frac{n\pi a}{b}\right)\right)^2.\end{aligned} \tag{72}$$

These two equations correspond exactly to Equations 12 and 13 of Humphreys' work once the difference in notation is taken into account.

Mathematical equivalence can also be demonstrated with the analytic solution for the ingrowth-diffusion equation under isothermal conditions (Wolf *et al.*, 1998, pp. 106-107). This time, letting the initial concentration be

$$c_n(0) = \overline{C}(0)\,\gamma_n\,, \tag{73}$$

a single time step of Eq. (35) results in

$$c_n(t) = c_n(0)\exp(-\mu_n\,Dt\,) + (\gamma_n\,Ut\,)\left(\frac{1-\exp(-\mu_n\,Dt\,)}{\mu_n\,Dt}\right). \tag{74}$$

Here a non-zero constant source term is explicitly included in the equation. As before, the total concentration is the sum over eigenfunction contributions,

$$\begin{aligned}\overline{C}(t) = \overline{C}(0)\sum_{n=1}^{\infty}\frac{6}{(n\pi)^2}\exp\left(-\frac{(n\pi)^2\,Dt}{a^2}\right) \\ + \frac{a^2 U}{D}\left(\frac{1}{15} - \sum_{n=1}^{\infty}\frac{6}{(n\pi)^4}\exp\left(-\frac{(n\pi)^2\,Dt}{a^2}\right)\right).\end{aligned} \tag{75}$$

In arriving at this last equation, the infinite series

$$\sum_{n=1}^{\infty}\frac{6}{(n\pi)^4} = \frac{6}{\pi^4}\zeta(4) = \frac{1}{15}\,, \tag{76}$$

is simplified using the well known Riemann-Zeta function,

$$\zeta(s) = \sum_{n=1}^{\infty} n^{-s}\,. \tag{77}$$

The properties of this function have been extensively studied, and tables exist for calculating its value for small integer arguments (Abramowitz and Stegun, 1972, pp. 807, 810-811). Eq. (75) corresponds exactly to Equation 5 of Wolf's work once it is multiplied by the source production rate and the difference in notation is taken into account.

Furthermore, in the limit of a large diffusion-time product Dt, the concentration in Eq. (75) approaches a steady-state value of

$$\overline{C}_{steady-state} = \frac{a^2 U}{15 D} = \frac{D_{steady-state}}{D}, \tag{78}$$

which corresponds to Humphreys' uniformitarian model once the difference in notation is taken into account (Humphreys, 2005a, p. 53, Equation 16). Considering the situation at hand, appropriate values are 20 μm for the radius of the diffusion domain and 1440 Ma for the reciprocal of the radioactive source function, assuming a constant source normalized to unity. Under these conditions, the steady-state diffusivity in Eq. (78) becomes

$$\begin{aligned} D_{steady-state} &= \frac{a^2 U}{15} = \frac{a^2}{15 t_{\max}} \\ &= \frac{(20\,\mu\text{m})^2}{15\,(1440\,\text{Ma})} \\ &= 5.87\times10^{-24}\ \text{cm}^2/\text{s}\,. \end{aligned} \tag{79}$$

Steady-state behavior is achieved if diffusivities are sustained well above this threshold value for the specified length of time. Conversely, diffusivities near or below this threshold value require non-steady-state models to accurately capture the time dependence. These exercises demonstrate the power of the method of Meesters and Dunai – Several different models which were published in the literature are actually special cases of the same general diffusion equation. Therefore, the method is not only a versatile computational engine, but it is also a powerful theoretical tool.

Finally, the projection of a solution from a given geometry onto a different geometry needs to be discussed. The primary motivation for solution projection is the desire to simulate a stepwise heating diffusion experiment starting with the final profile from a simulation of a sample's prior geologic history. If a zoned model is used to represent the shell of biotite surrounding a zircon core, as in Humphreys' creation model, then the final solution with the shell must be projected onto a new set of basis functions for a bare zircon prior to simulating the heating steps of the experiment. The projection proceeds in a straight forward manner. The main item to note is that the coefficients for the actual spatial concentration f_n and not the coefficients for the average concentration over volume c_n must be used (see Eq. (21) and the surrounding discussion for details),

$$f'_n = \sum_m P_{nm}\, f_m\,. \tag{80}$$

Here f_m and f'_n are the spatial concentration coefficients for the initial and final geometries respectively, and P_{nm} is the projection matrix which is defined as

$$P_{nm} = \frac{\int u'_n(x,y,z)\, u_m(x,y,z)\, dV}{\int u'^2_n(x,y,z)\, dV}\,. \tag{81}$$

For the case of spherical geometry, this equation simplifies to

$$\begin{aligned} P_{nm} &= \frac{\int_0^{a'} \sin(k'_n r)\sin(k_m r)\, dr}{\int_0^{a'} \sin^2(k'_n r)\, dr} \\ &= \begin{cases} 1 & \text{if } k'_n = k_m \\ \dfrac{\mathrm{I_X}(a';k'_n,k_m)}{\mathrm{I_S}(a';k'_n)} & \text{if } k'_n \neq k_m \end{cases}. \end{aligned} \tag{82}$$

Although the projection is straight forward and easy to implement, it is actually fairly computationally expensive. If N eigenfunctions are used for both geometries, the total number of mathematical operations will be on the order of N^2. Using the same numbers as in the previous example, for 10 000 eigenfunctions, on the order of 100 000 000 mathematical operations will be required. The solution projection often takes longer than the diffusion simulation!

B.3. Numerical results

Before applying the diffusion method to cases of geologic interest, several simpler systems were studied in order to better understand the algorithm and gain confidence with the technique. In particular, problems with analytic solutions were investigated because they impose a rigorous check on not only the diffusion algorithm itself, but also on its implementation in the Python programming language.

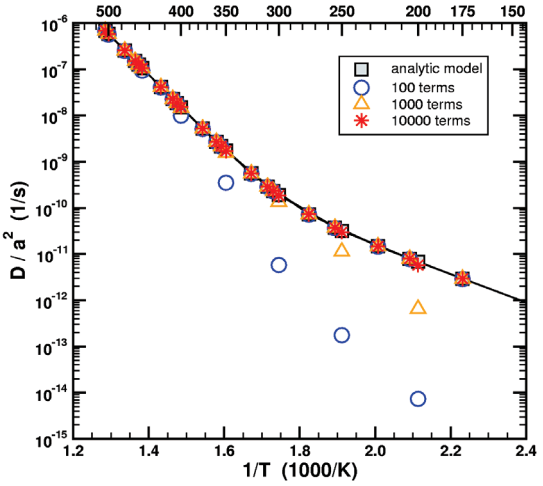

Figure 15. Simulation of an idealized stepwise heating experiment in which an analytic model is compared to numerical models using 100, 1000, and 10 000 eigenfunction terms in the series expansion. Good agreement between the analytic model and the numerical model is obtain when 10 000 terms are used.

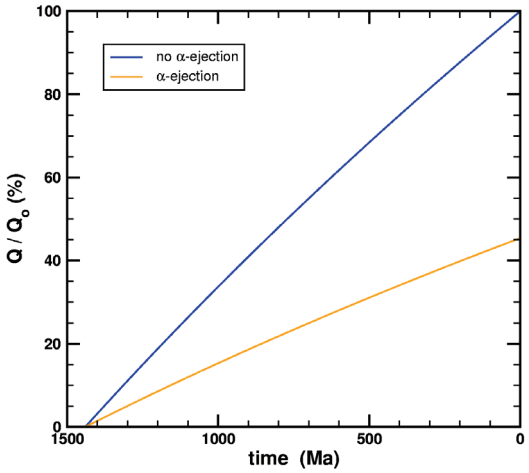

Figure 17. Simulation of the growth of helium over time without any diffusion loss. The source function of Fig. 16 was used in a 20 µm spherical model. The curve without a correction for α-ejection reaches unity over a time of 1440 Ma. The final value drops to only 45% once a correction is made for α-ejection using a mean particle range of 15.3 µm. The time convention uses zero for the present age and positive numbers for time before present.

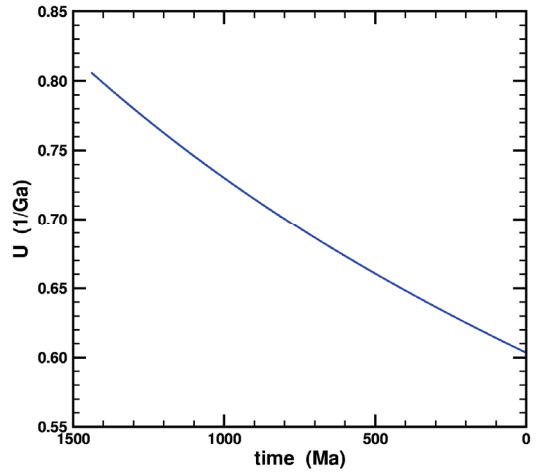

Figure 16. Time dependent source function for helium generated by radioactive decay from ^{238}U, ^{235}U, and ^{232}Th in a 10:1:1 concentration ratio. The normalization of the function is such that the integral over a 1440 Ma time span is unity. The time convention uses zero for the present age and positive numbers for time before present.

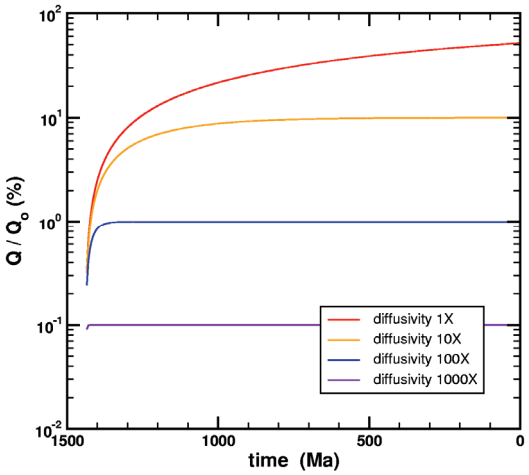

Figure 18. Simulation of the simultaneous generation and diffusion of helium. A constant source function normalized to unity over a time of 1440 Ma was used in a 20 µm spherical model. The diffusivity for each curve is expressed as a multiple of the threshold value for steady-state behavior. The time convention uses zero for the present age and positive numbers for time before present.

The first case considered was an idealized stepwise heating diffusion experiment. Using a model diffusivity of

$$D(T) = 1.40\times10^{-1}\ \exp\left(\frac{-38.1\ \text{kcal/mol}}{RT}\right) + 7.40\times10^{-11}\exp\left(\frac{-13.9\ \text{kcal/mol}}{RT}\right)\ \text{cm}^2/\text{s}\,, \tag{83}$$

the real Fenton Hill zircon diffusion experiment of Fig. 2 was emulated. The expected gas loss from a 20 μm zircon sphere was calculated using Equation 4b of Fechtig and Kalbitzer, after which Equation 5b was used to calculate the diffusivity (Fechtig and Kalbitzer, 1966, pp. 70-72). Since these equations are algebraic inverses of each other, the calculated diffusivity was identical to the model diffusivity initially used for the experiment. This procedure was repeated using the numerical method to calculate the gas loss at each heating step instead of the analytic equation. The diffusion models made no correction for α-particle ejection and assumed no radioactive source (see Eqs. (49)-(52)). A uniform initial profile was assumed. Fig. 15 shows the results of this idealized experiment for numerical models with 100, 1000, and 10 000 eigenfunction terms. Only the model with 10 000 terms is in good agreement with the analytic model over the entire temperature range.

In order to test the growth capabilities of the algorithm, a case was studied in which helium produced by radioactive decay accumulated without loss due to diffusion. In Fig. 16 the time-dependent source function of Eq. (8) is plotted over a time period of 1440 Ma. This source function was then used in a 20 μm spherical model to simulate the growth of helium over time without any diffusion loss (Fig. 17). By comparing simulations both with and without a correction for α-particle ejection, the mean α-particle range could be determined. (See section 4.5).

Finally, the case of simultaneous generation and diffusion was tested by selecting simulation conditions for which the limit predicted by Eq. (78) would be achieved. A constant source function normalized over 1440 Ma was used in a 20 μm spherical model so that the steady-state diffusivity threshold given by Eq. (79) would apply. The helium diffusivities were set at multiples of 1×, 10×, 100×, and 1000× times this threshold value. Under these circumstances, the concentration ratios are expected to asymptotically approach values of 100%, 10%, 1%, and 0.1% respectively. The correct asymptotic limits were achieved for the three cases with the highest diffusivity (Fig. 18). The 1× diffusivity case was not expected to reach its asymptotic value.

The significance of these idealized studies is that both the derivation and implementation of the diffusion method were rigorously tested in three important cases which have analytic solutions:

1. Helium diffusion without generation for an arbitrary and abruptly changing temperature history.
2. Helium generation without diffusion for an arbitrary source function, both with and without a correction for α-ejection.
3. Simultaneous generation and diffusion of helium for a constant temperature and source function.

Because of these successful results, greater confidence can be placed in applying the method to more complicated problems of geologic interest for which analytic solutions do not exist.

Appendix C. Stepwise heating experiment

In addition to simulating the helium retention ratio as a function of depth down the geothermal test wells, the diffusion model was also applied to analyzing a stepwise heating experiment using zircon samples from well GT-2 (Humphreys *et al.,* 2004). The procedure of Fechtig and Kalbitzer is often used to extract the temperature dependent diffusivities from the gas released at each step in such an experiment (1966). Although this method is popular because the diffusivities can be calculated from a closed form analytic expression, there are several limitations. First, the mathematical assumptions of the method require a spatially uniform concentration profile. This condition is violated by these zircons because of both α-particle ejection and diffusive loss. Second, the method assumes that all the gas is derived from a single diffusion domain (Shuster *et al.*, 2005). The diffusivities that are calculated are no longer valid if diffusion occurs in multiple domains, especially for the lower temperatures of the experiment.

In principle, the technique of Meesters and Dunai (2002a and 2002b) can be used to extract the diffusivities from a stepwise heating experiment. Because the method is quite general, no restrictions

on the initial concentration profile or diffusion kinetics are imposed. However, no analytic formula exists for calculating the diffusivities from the gas release. This information, though, can be obtained using nonlinear optimization. In fact, if the initial concentration profile is simulated assuming a given thermal history, its shape is dependent upon the diffusivities that are to be extracted from the experimental data, and the optimization loop must include both the geologic history in addition to the heating schedule of the experiment for self-consistency. Although this approach may sound unreasonable, it turns out to be quite feasible in practice, with total computer times on the order of minutes for optimization of a given experiment. (See Loechelt *et al.*, 1993, for an example of a diffusion experiment that used nonlinear optimization in the extraction of kinetic parameters.)

The nonlinear optimization algorithm was implemented in the following fashion. Using a trial set of diffusion coefficients with a fixed partitioning of gas between the HRD and LRD, a simulation was performed for a given thermal history, generating the initial profile for the laboratory experiment. The incremental gas release from each step in the heating schedule of this experiment was simulated using the same diffusion coefficients, thereby guaranteeing self-consistency. The stepwise gas losses were then analyzed using the analytic formula of Fechtig and Kalbitzer (1966) and compared to the measured diffusivities, excluding the initial heating ramp. A least squares error quantity was calculated from the logarithm of the diffusivity ratios at each temperature step and used by a downhill simplex algorithm to adjust the diffusion parameters (Press *et al.*, 1988). This process was iterated until convergence was observed. The first iteration of the optimization loop started with the diffusivities from Eq. (83), which were obtained from the experimental data using the analytic formula of Fechtig and Kalbitzer.

Figure 19 compares the results of the simulated stepwise heating experiment to the measured data. By construction, the nonlinear optimization forces agreement between simulation and measurement after the first 9 steps of the initial heating ramp. However, the simulations match the measured data well even for this initial unconstrained portion of the experiment, indicating that the underlying thermal history and diffusion kinetics are at least consistently if not uniquely determined. The multi-domain diffusion model (Eqs. (6)-(7)) assigns a gas fraction

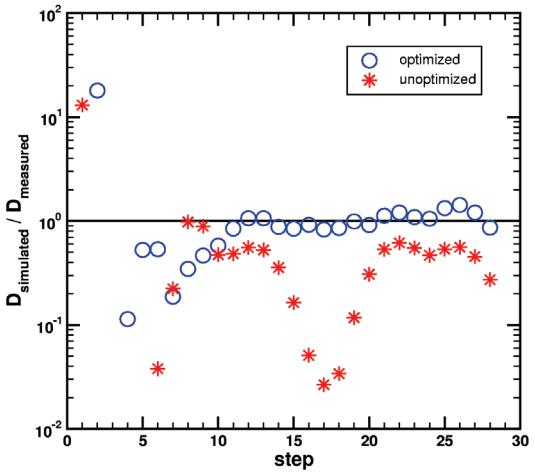

Figure 19. Ratio of simulated to measured helium diffusivities extracted from a stepwise heating experiment. The simulations were performed using a parameter set that was self-consistently optimized for the old-earth model (Eqs. (6)-(7)). Simulations with the initial unoptimized parameter set are shown for comparison (Eq. (83)).

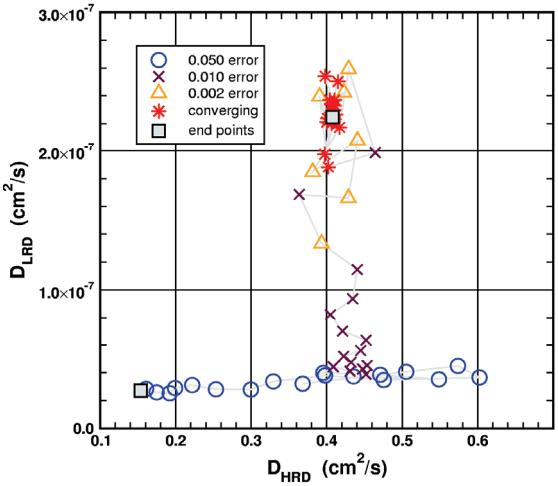

Figure 20. The convergence trajectory of the nonlinear optimizer in the diffusion parameter space. The two independent variables are the diffusion coefficients for the *high retentivity domain* (HRD) and the *low retentivity domain* (LRD).

of 0.3% to the LRD. This value is not well constrained by the experimental data, and reasonable fits could be obtained for fractions ranging from 0.1% to 10%, with the quality of fit deteriorating rapidly for values less than 0.1%. A single stepwise heating experiment can only provide a limited constraint on the kinetics of possible multi-domain diffusion models.

A final point of interest is the convergence properties of the nonlinear optimization itself. Figure 20 shows the trajectory of the optimizer in the diffusion parameter space. Two orthogonal paths are apparent. The optimization sequence is first dominated by the diffusivity for the HRD at the higher temperature steps of the experiment. After this parameter converges, the simplex moves orthogonally to find the diffusivity for the LRD.

Epilogue

The RATE researchers have compared their efforts to the struggle between David and Goliath (Vardiman *et al.*, 2000, pp. 24-25). The young-earth creationist community often comments about their disadvantage when compared to their secular scientific counterparts. They have no government funding and no support from large institutions. Despite these handicaps, the RATE program still managed to solicit gifts and donations in excess of $1,250,000 for their research activities (Vardiman *et al.*, 2005, pp. 4-5).

Regardless of what the RATE scientists may think about me and my work, they should be relieved to know that they are not competing against a large institution or government agency. This work was conducted on my personal time outside of my professional employment as an electrical engineer in the semiconductor industry. All of the expenses, which were mostly for books and papers, were paid for out of my own pocket.

Furthermore, the young-earth creationist community publishes most of their works outside of the scientific mainstream in their own journals and conferences, oftentimes claiming that the scientific majority has excluded their point-of-view from consideration. Therefore, in an attempt to determine how open their forums are to outside criticism, I submitted an earlier version of this work to one of their own journals: the Creation Research Society Quarterly. Unfortunately, it was ultimately rejected by the physics section editor after a painful, and in my opinion, unfair review process. I am deeply grateful to Reasons to Believe and their staff for encouraging me to continue this work after it was rejected by the CRSQ, and for providing a venue for sharing these results with the public.

References

Abramowitz, M., Stegun, I.A., 1972. Handbook of Mathematical Functions with Formulas, Graphs, and Mathematical Tables, Tenth Printing, U.S. Government Printing Office, Washington, DC.

Armstrong, A.K., Mamet, B.L., Repetski, J.E., 2004. Mississippian system of New Mexico and adjacent areas. In the Geology of New Mexico, a Geologic History, Mack, G.H., Giles, K.A. (Ed.), New Mexico Geological Society, Special Publication 11:77-93.

Austin, S.A., 1994. Are Grand Canyon rocks one billion years old? In Grand Canyon: Monument to Catastrophe, Austin, S.A. (Ed.), Institute for Creation Research, Santee, CA, Chapter 6, pp. 111-131.

Austin, S.A., Snelling, A.A., 1998. Discordant potassium-argon model and isochron "ages" for Cardenas Basalt (middle Proterozoic) and associated diabase of eastern Grand Canyon, Arizona. In Proceedings of the Fourth International Conference on Creationism, Walsh, R.E. (Ed.), Creation Science Fellowship, Pittsburgh, PA, pp. 35-51.

Baldridge, W.S., 2004. Geology of the American Southwest: A Journey through Two Billion Years of Plate-Tectonic History, Cambridge University Press, Cambridge, United Kingdom.

Baltz, E.H., Myers, D.A., 1999. Stratigraphic framework of upper Paleozoic rocks, southeastern Sangre de Cristo Mountains, New Mexico with a section on speculations and implications for regional interpretation of Ancestral Rocky Mountains paleotectonics, New Mexico Bureau of Geology & Mineral Resources Memoir 48:1-269.

Baum, E.M., Knox, H.D., Miller, T.R., 2002. Nuclides and Isotopes, Sixteenth Edition, Knolls Atomic Power Laboratory, Schenectady, NY.

Beazley, D.M., 2000. Python Essential Reference, New Riders Publishing, Indianapolis, IN.

Bell, R.P., 1945. A problem of heat conduction with spherical symmetry, Proceedings of the Physical Society (London), 57:45-48.

Brookins, D.G., Forbes, R.B., Turner, D.L., Laughlin, A.W., Naeser, C.W., 1977. Rb-Sr, K-Ar, and fission-track geochronological studies of samples from LASL drill holes GT-1, GT-2, and EE-1, Los Alamos National Laboratories, Report LA-6829-MS:1-27.

Brookins, D.G., Laughlin, A.W., 1983. Rb-Sr geochronologic investigation of Precambrian samples from deep geothermal drill holes, Fenton Hill, New Mexico, Journal of Volcanology and Geothermal Research 15:43-58.

Cather, S.M., 2004. Laramide orogeny in central and northern New Mexico and southern Colorado. In the Geology of New Mexico, a Geologic History, Mack, G.H., Giles, K.A. (Ed.), New Mexico Geological Society, Special Publication 11:203-248.

Cook, M.A., 1968. Radiological dating and some pertinent applications of historical interest: do radiological "clocks" need repair? Creation Research Society Quarterly 5:69-77.

Dalrymple, G.B., 1991. The Age of the Earth, Stanford University Press, Stanford, CA.

DeYoung, D., 2005. Thousands not Billions: Challenging an Icon of Evolution, Master Books, Green Forest, AR.

Dickin, A.P., 1995. Radiogenic Isotope Geology, Cambridge University Press, Cambridge, United Kingdom.

Dunai, T.J., 2005. Forward modeling and interpretation of (U-Th)/He ages. In Reviews in Mineralogy and Geochemistry, Reiners, P.W., Ehlers, T.A. (Ed.), The Mineralogical Society of America, Chantilly, VA, 58:259-274.

Farley, K.A., 2002. (U-Th)/He dating: techniques, calibrations, and applications. In Reviews in Mineralogy and Geochemistry, Porcelli, D., Ballentine, C.J., Wieler, R. (Ed.), The Mineralogical Society of America, Washington, DC, 47:819-843.

Fechtig, H., Kalbitzer, S., 1966. The diffusion of argon in potassium-bearing solids. In Potassium Argon Dating, Schaeffer, O.A., Zähringer, J. (Ed.), Springer-Verlag, New York, pp. 68-107.

Fitzgerald, P.G., Baldwin, S.L., Webb, L.E., and O'Sullivan, P.B., 2006. Interpretation of (U-Th)/He single grain ages from slowly cooled crustal terranes, a case study from the Transantarctic Mountains of southern Victoria Land, Chemical Geology 225:91-120.

Foeken, J.P.T., Persano, C., Stuart, F.M., and ter Voorde, M., 2007. Role of topography in isotherm perturbation, apatite (U-Th)/He and fission track results from the Malta tunnel, Tauern Window, Austria, Tectonics 26 (TC3006):1-15.

Formento-Trigilio, M.L., and Pazzaglia, F.J., 1998. Tectonic geomorphology of the Sierra Nacimiento: traditional and new techniques in assessing long-term landscape evolution in the Southern Rocky Mountains, Journal of Geology, 106:433-453.

Gardner, J.N., Goff, F., Garcia, S., Hagan, R.C., 1986. Stratigraphic relations and lithologic variations in the Jemez Volcanic Field, New Mexico, Journal of Geophysical Research 91(B2):1763-1778.

Gentry, R.V., Glish, G.L., McBay, E.H., 1982a. Differential helium retention in zircons: implications for nuclear waste containment, Geophysical Research Letters 9 (10):1129-1130.

Gentry, R.V., Sworski, T.J., McKown, H.S., Smith, D.H., Eby, R.E., Christie, W.H., 1982b. Differential lead retention in zircons: implications for nuclear waste containment, Science 216:296-298.

Gill, G.H., 1996. A sufficient reason for false Rb-Sr isochrons, Creation Research Society Quarterly 33:105-108.

Goff, F., Gardner, J.N., 2004. Late Cenozoic geochronology of volcanism and mineralization in the Jemez Mountains and Valles caldera, north central New Mexico. In the Geology of New Mexico, a Geologic History, Mack, G.H., Giles, K.A. (Ed.), New Mexico Geological Society, Special Publication 11:295-312.

Greenfield, P., Miller, T., White, R., Hsu, J.C., Barrett, P., Küpper, J., Verveer, P.J., 2005. numarray User's Manual, Release 1.5, Space Telescope Science Institute, Baltimore, MD.

Harrison, T.M., Morgan, P., Blackwell, D.D., 1986. Constraints on the age of heating at the Fenton Hill site, Valles caldera, New Mexico, Journal of Geophysical Research 91(B2):1899-1908.

Helmick, L.S., Baumann, D.P., 1989. A demonstration of the mixing model to account for Rb-Sr isochrons, Creation Research Society Quarterly 26:20-23.

Humphreys, D.R., 2000. Accelerated nuclear decay: a viable hypothesis? In Vardiman *et al.* (2000), Chapter 7, pp. 333-379.

Humphreys, D.R., Austin, S.A., Baumgardner, J.R., Snelling, A.A., 2003a. Recently measured helium diffusion rate for zircon suggests inconsistency with U-Pb age for Fenton Hill granodiorite, EOS, Transactions of the American Geophysical Union, 84 (46), Fall Meeting Supplement, abstract V32C-1047.

Humphreys, D.R., Austin, S.A., Baumgardner, J.R., Snelling, A.A., 2003b. Helium diffusion rates support accelerated nuclear decay. In Proceedings of the Fifth International Conference on Creationism, Ivey, Jr., R.L. (Ed.), Creation Science Fellowship, Pittsburgh, PA, pp. 175-195.

Humphreys, D.R., Austin, S.A., Baumgardner, J.R., Snelling, A.A., 2004. Helium diffusion age of 6,000 years supports accelerated nuclear decay, Creation Research Society Quarterly 41:1-16.

Humphreys, D.R., 2005a. Young helium diffusion age of zircons supports accelerated nuclear decay. In Vardiman *et al.* (2005), Chapter 2, pp. 25-100.

Humphreys, D.R., 2005b. Helium evidence for a young world remains crystal-clear, Institute for Creation Research, El Cajon, CA, http://www.icr.org/pdf/rate/humphreys_to_hanke.pdf

Karlstrom, K.E., Amato, J.M., Williams, M.L., Heizler, M., Shaw, C.A., Read, A.S., Bauer, P., 2004. Proterozoic tectonic evolution of the New Mexico region: a synthesis. In the Geology of New Mexico, a Geologic History, Mack, G.H., Giles, K.A. (Ed.), New Mexico Geological Society, Special Publication 11:1-34.

Kelley, S.A., Chapin, C.E., Corrigan, J. 1992. Late Mesozoic to Cenozoic cooling histories of the flanks of the northern and central Rio Grande rift, Colorado and New Mexico, New Mexico Bureau of Geology & Mineral Resources Bulletin 145:1-39.

Kelley, S.A., Osburn, G.R., Kempter, K.A., 2007. Geology of Cañon de San Diego, southwestern Jemez Mountains, north-central New Mexico. In Geology of the Jemez Region II, Kues, B.S., Kelley, S.A., Lueth, V.W. (Ed.), New Mexico Geological Society, Guidebook 58:169-181.

Kirstein, L.A., Sinclair, H., Stuart, F.M., and Dobson, K., 2006. Rapid early Miocene exhumation of the Ladakh batholith, western Himalaya, Geology 34 (12):1049-1052.

Kolstad, C.D., McGetchin, T.R., 1978. Thermal evolution models for the Valles caldera with reference to a hot-dry-rock geothermal experiment, Journal of Volcanology and Geothermal Research 3:197-218.

Kues, B.S., Giles, K.A., 2004. The late Paleozoic Ancestral Rocky Mountains system in New Mexico. In the Geology of New Mexico, a Geologic History, Mack, G.H., Giles, K.A. (Ed.), New Mexico Geological Society, Special Publication 11:95-136.

Laughlin, A.W., Eddy, A.C., Laney, R., Aldrich, Jr., M.J., 1983. Geology of the Fenton Hill, New Mexico hot dry rock site, Journal of Volcanology and Geothermal Research 15:21-41.

Loechelt, G.H., Tam, G., Steele, J.W., Knoch, L.K., Klein, K.M., Watanabe, J.K., Christiansen, J.W., 1993. Measurement and modeling of boron diffusion in Si and strained $Si_{1-x}Ge_x$ epitaxial layers during rapid thermal annealing, Journal of Applied Physics 74 (9):5520-5526.

Lorencak, M., Kohn, B.P., Osadetz, K.G., Gleadow, A.J.W., 2004. Combined apatite fission track and (U-Th)/He thermochronometry in a slowly cooled terrane: results from a 3440-m-deep drill hole in the southern Canadian Shield, Earth and Planetary Science Letters 227:87-104.

Lucas, S.G., 2004. The Triassic and Jurassic systems in New Mexico. In the Geology of New Mexico, a Geologic History, Mack, G.H., Giles, K.A. (Ed.), New Mexico Geological Society, Special Publication 11:137-152.

McMillan, N.J., McLemore, V.T., 2004. Cambrian-Ordovician magmatism and extension in New Mexico and Colorado, New Mexico Bureau of Geology & Mineral Resources Bulletin 160:1-11.

Meesters, A.G.C.A., Dunai, T.J., 2002a. Solving the production-diffusion equation for finite diffusion domains of various shapes. Part I: implications for low-temperature (U-Th)/He thermochronology, Chemical Geology 186:333-344.

Meesters, A.G.C.A., Dunai, T.J., 2002b. Solving the production-diffusion equation for finite diffusion domains of various shapes. Part II: applications to cases with α–ejection and nonhomogeneous distribution of the source, Chemical Geology 186:347-363.

Morris, H.M., 1974. Scientific Creationism, Master Books, Green Forest, AR, Chapter 6, pp. 137-149.

Morris, J.D., 1994. The Young Earth, Master Books, Green Forest, AR, Chapter 5, pp. 51-67.

Myrow, P.M., Taylor, J.F., Miller, J.F., Ethington, R.L., Ripperdan, R.L., Allen, J., 2003. Fallen arches: dispelling myths concerning Cambrian and Ordovician paleogeography of the Rocky Mountain region, GSA Bulletin, 115:695-713.

Nummedal, D., 2004. Tectonic and eustatic controls on upper Cretaceous stratigraphy of northern New Mexico. In the Geology of New Mexico, a Geologic History, Mack, G.H., Giles, K.A. (Ed.), New Mexico Geological Society, Special Publication 11:169-182.

Oliphant, T.E., 2006. Guide to NumPy, Sponsored by Enthought, http://www.scipy.org/Documentation.

Pazzaglia, F.J., Kelley, S.A., 1998. Large-scale geomorphology and fission-track thermochronology in topographic and exhumation reconstructions of the Southern Rocky Mountains, Rocky Mountain Geology, 33:229-257.

Persano, C., Stuart, F.M., Bishop, P., Dempster, T.J., 2005. Deciphering continental breakup in eastern Australia using low-temperature thermochronometers, Journal of Geophysical Research 110 (B12405):1-17.

Press, W.H., Flannery, B.P., Teukolsky, S.A., Vetterling, W.T., 1988. Numerical Recipes in C, Cambridge University Press, Cambridge, United Kingdom, pp. 305-309.

Purtymun, W.D., West, F.G., Pettitt, R.A., 1974. Geology of geothermal test hole GT-2, Fenton Hill site, July 1974, Los Alamos National Laboratories, Report LA-5780-MS:1-15.

Reiners, P.W., Farley, K.A., 1999. Helium diffusion and (U-Th)/He thermochronometry of titanite, Geochimica et Cosmochimica Acta 63 (22):3845-3859.

Reiners, P.W., Spell, T.L., Nicolescu, S., Zanetti, K.A., 2004. Zircon (U-Th)/He thermochronometry: He diffusion and comparisons with 40Ar/39Ar dating, Geochimica et Cosmochimica Acta 68 (8):1857-1887.

Reiners, P.W., 2005. Zircon (U-Th)/He thermochronometry. In Reviews in Mineralogy and Geochemistry, Reiners, P.W., Ehlers, T.A. (Ed.), The Mineralogical Society of America, Chantilly, VA, 58:151-179.

Reiter, M., 2007. Geophysical studies relating to the geothermal source of the Valles caldera, north-central New Mexico. In Geology of the Jemez Region II, Kues, B.S., Kelley, S.A., Lueth, V.W. (Ed.), New Mexico Geological Society, Guidebook 58:78-80.

Sanders, R.E., Heizler, M.T., Goodwin, L.B., 2006. 40Ar/39Ar thermochronology constraints on the timing of Proterozoic basement exhumation and fault ancestry, southern Sangre de Cristo Range, New Mexico, GSA Bulletin, 118:1489-1506.

Shuster, D.L., Farley, K.A., Sisterson, J.M., Burnett, D.S., 2003. Quantifying the diffusion kinetics and spatial distributions of radiogenic 4He in minerals containing proton-induced 3He, Earth and Planetary Science Letters 217:19-32.

Shuster, D.L., Vasconcelos, P.M., Heim, J.A., Farley, K.A., 2005. Weathering geochronology by (U-Th)/He dating of goethite, Geochimica et Cosmochimica Acta 69 (3):659-673.

Slusher, H.S., 1973. Critique of Radiometric Dating, Institute for Creation Research, San Diego, CA.

Smith, R.L., Bailey, R.A., and Ross, C.S., 1970. Geologic map of the Jemez Mountains, New Mexico, U.S. Geological Survey, Miscellaneous Geological Investigations Map 1-571, scale 1:250,000.

Smith, G.A., 2004. Middle to late Cenozoic development of the Rio Grande Rift and adjacent regions in northern New Mexico. In the Geology of New Mexico, a Geologic History, Mack, G.H., Giles, K.A. (Ed.), New Mexico Geological Society, Special Publication 11:331-358.

Snelling, A.A., Baumgardner, J.R., Vardiman, L., 2003a. Abundant Po radiohalos in Phanerozoic granites and timescale implications for their formation, EOS, Transactions of the American Geophysical Union, 84 (46), Fall Meeting Supplement, abstract V32C-1046.

Snelling, A.A., Armitage, M.H., 2003b. Radiohalos – a tale of three granitic plutons. In Proceedings of the Fifth International Conference on Creationism, Ivey, Jr., R.L. (Ed.), Creation Science Fellowship, Pittsburgh, PA, pp. 243-267.

Snelling, A.A., 2005. Radiohalos in granites: evidence for accelerated nuclear decay. In Vardiman *et al.* (2005), Chapter 3, pp. 101-207.

Söderlund, P., Juez-Larré, J., Page, L., and Dunai, T., 2005. Extending the time range of apatite (U-Th)/He thermochronometry in slowly cooled terranes, Paleozoic to Cenozoic exhumation history of southeast Sweden, Earth and Planetary Science Letters 239:266-275.

Steiger, R.H., Jäger, E., 1977. Subcommission on geochronology: convention on the use of decay constants in geo- and cosmochronology, Earth and Planetary Science Letters 36:359-362.

Woodmorappe, J., 1999. The Mythology of Modern Dating Methods, Institute for Creation Research, El Cajon, CA.

Woodward, L.A., 1987. Geology and mineral resources of Sierra Nacimiento and vicinity, New Mexico, New Mexico Bureau of Geology & Mineral Resources Memoir 42:1-84.

Vardiman, L., Snelling, A.A., Chaffin, E.F. (Ed.), 2000. Radioisotopes and the Age of the Earth, Volume I: A Young-Earth Creationist Research Initiative, Institute for Creation Research, El Cajon, CA, and the Creation Research Society, St. Joseph, MO.

Vardiman, L., Snelling, A.A., Chaffin, E.F. (Ed.), 2005. Radioisotopes and the Age of the Earth, Volume II: Results of a Young-Earth Creationist Research Initiative, Institute for Creation Research, El Cajon, CA, and the Creation Research Society, Chino Valley, AZ.

Vermeesch, P., Seward, D., Latkoczy, C., Wipf, M., Günther, D., and Baur, H., 2007. α-Emitting mineral inclusions in apatite, their effect on (U-Th)/He ages, and how to reduce it, Geochimica et Cosmochimica Acta 71:1737-1746.

Wolf, R.A., Farley, K.A., Kass, D.M., 1998. Modeling of the temperature sensitivity of the apatite (U-Th)/He thermochronometer, Chemical Geology 148:105-114.

Zartman, R.E., 1979. Uranium, thorium and lead concentrations and lead isotopic composition of biotite granodiorite (sample 9527-2b) from LASL drill hole GT-2, Los Alamos National Laboratories, Report LA-7923-MS:1-18.